2007

ASYMMETRIC SIMPLE EXCLUSION PROCESS IN TWO DIMENSIONS

Dmytro Goykolov
University of Kentucky, goykolov@uky.edu

ABSTRACT OF DISSERTATION

Dmytro Goykolov

The Graduate School

University of Kentucky

2007

ASYMMETRIC SIMPLE EXCLUSION PROCESS IN TWO DIMENSIONS

ABSTRACT OF DISSERTATION

A dissertation submitted in partial fulfillment of the
requirements for the degree of Doctor of Phylosophy in the
College of Arts and Sciences
at the University of Kentucky

By

Dmytro Goykolov

Lexington, Kentucky

Director: Dr. Joseph Straley, Professor of Physics,

Department of Physics and Astronomy

Lexington, Kentucky

2007

ABSTRACT OF DISSERTATION

ASYMMETRIC SIMPLE EXCLUSION PROCESS IN TWO DIMENSIONS

Asymmetric simple exclusion process (ASEP) is a driven stochastic lattice model of particles that move preferentially in one direction. If particles move only in one direction, the model is known as totally asymmetric process. Conventionally, preferred direction of motion is chosen to be to the right. Particles interact through the hard core exclusion rule, meaning that no more than one particle is allowed to occupy one lattice site.

In this work following ASEP models are presented. First we study square diagonal lattice with particles that occupy one lattice site and move along the square diagonals. Mean-field theory was developed for this model. The results that were obtained are the dependency of the current on density of the particles, spatial density distribution along the horizontal direction and the phase diagram of the system. Mean-field theory results were compared to simulations.

Next model was lattice with extended particles, i.e. particles that occupy more than one lattice site. Unlike the first model, in this system the particle-hole symmetry is broken. Results for current flow, density distribution and phase diagrams were obtained both by mean-field theory and Monte-Carlo (MC) simulations.

Another system was the lattice with vertical particle drift. Now particles that occupy one lattice site jump not only in one preferred horizontal directions but there is also one preferred vertical direction for particle flow. Both mean-field theory and simulations were studied for this system and results were compared.

Also we explore the system with immovable obstacle. Obstacle is one or several particles located at fixed positions. In this model we observe increase in particle density in front of the obstacle and "shadow" behind it. It is expected that the shape and size of those formations are symmetrical in transverse direction.

KEYWORDS: 2D ASEP, Phase Diagram, 2D ASEP with Extended Particles, 2D ASEP with vertical bias, 2D ASEP with an Obstacle

Dmytro Goykolov

February 21, 2007

ASYMMETRIC SIMPLE EXCLUSION PROCESS

By
Dmytro Goykolov

Joseph Straley
Director of Dissertation

Tom Troland
Director of Graduate Studies

February 21, 2007

RULES FOR THE USE OF DISSERTATION

Unpublished dissertations submitted for the Master's and Doctor's degrees and deposited in the University of Kentucky Library are as a rule open for inspection, but are to be used only with due regard to the rights of the authors. Bibliographical references may be noted, but quotations or summaries of parts may be published only with the permission of the author, and with the usual scholarly acknowledgments.

Extensive copying or publication of the dissertation in whole or in part requires also the consent of the Dean of the Graduate School of the University of Kentucky.

A library which borrows this dissertation for use by its patrons is expected to secure the signature of each user.

Name **Date**

_____

_____

_____

_____

_____

_____

_____

_____

_____

_____

_____

_____

_____

_____

_____

_____

_____

DISSERTATION

Dmytro Goykolov

The Graduate School

University of Kentucky

2007

ASYMMETRIC SIMPLE EXCLUSION PROCESS IN TWO DIMENSIONS

DISSERTATION

A dissertation submitted in partial fulfillment of the
requirements of the degree of Doctor of Phylosophy in the
College of Arts and Sciences
at the University of Kentucky

By

Dmytro Goykolov

Lexington, Kentucky

Director: Dr. Joseph Straley, Professor of Physics,

Department of Physics and Astronomy

Lexington, Kentucky

2007

Contents

List of Figures v

List of Files vii

Chapter 1. Introduction 1

Chapter 2. Definition of the Models 7

2.1 One Dimensional Model. 7
2.1.1 Definition of the Model. 7
2.1.2 Phase Diagram for the One Dimensional Model. 8
2.2 Two-Dimensional Model 11

Chapter 3. Two-Dimensional Model 13

3.1 Mean-Field Theory for Regions Far From Critical. 13
3.2 The Case of Transverse Symmetry and Steady State. 14
3.3 Simulation Results and Comparison with the MFT. 16
3.4 Coexistence Line. 28

Chapter 4. Extended Particles (Breaking the Particle-Hole Symmetry) 33

4.1 Mean-Field Theory 33
4.1.1 Horizontally Extended Particles. 33
4.1.2 Vertically Extended Particles. 37
4.2 Simulation Results. 38
4.2.1 Horizontally Extended Particles. 38
4.2.2 Vertically Extended Particles. 42

Chapter 5. 2D ASEP Model with Vertical Particle Drift 47

5.1 Mean-Field Theory. 47
5.2 Simulation Results 51
5.2.1 50x50 lattice. 51
5.2.2 100x100 lattice. 52
5.2.3 200x200 lattice. 55

Chapter 6. Lattice with an Obstacle 58

6.1 Mean-field theory 58
6.2 Simulation Results 61

Chapter 7. Summary 64

Appendices 67

Appendix A. Details of the Monte Carlo Model 67

A.1. Regular 2D Model 67
A.2. Regular Model With Periodic Lattice 69
A.3. Extended Particles 71
A.3. Vertical Drift Model 72
A.4. Model with the Obstacle 73
A.5. Random Number Generator 74
A.6. Technical Details 74

Bibliography 75

Vita 77

List of Figures

1.1 Structure of ZSM-5 zeolite. 2

2.1 One-dimensional ASEP model. 7
2.2 Phase diagram for the one dimensional ASEP model. 9
2.3 Dependency of the current on the bulk density of the particles in one-dimensional ASEP model. 10
2.4 Two-dimensional ASEP model. 11
2.5 Coordinate system and labeling of the sites. 12

3.1 Density distribution along the y axis in the periodic 100x100 lattice. . 18
3.2 Average current vs time in the 50x50 system with dominating low density phase. 18
3.3 Average current vs time in the 100x100 system with dominating low density phase. 19
3.4 Average current vs time in the 200x200 system with dominating low density phase. 19
3.5 Density profiles in the 50x50 system with dominating low density phase 20
3.6 Density profiles in the 100x100 system with dominating low density phase 20
3.7 Density profiles in the 200x200 system with dominating low density phase 21
3.8 Density profiles in the 50x50 system with dominating high density phase 22
3.9 Density profiles in the 100x100 system with dominating high density phase 23
3.10 Density profiles in the 200x200 system with dominating high density phase 23
3.11 Density profile for the maximal current phase in 50x50 lattice. 24
3.12 Density profile for the maximal current phase in 100x100 lattice. . . . 25
3.13 Density profile for the maximal current phase in 200x200 lattice. . . . 25
3.14 Current vs density plot for the 50x50 lattice. 26
3.15 Current vs density plot for the 100x100 lattice. 27
3.16 Current vs density plot for the 200x200 lattice. 27
3.17 Open 100x100 system at the coexistence line. Data from 6 independent runs. 28
3.18 Open 200x200 system at the coexistence line. Data from 6 independent runs. 29
3.19 Density profile of the periodic 50x50 lattice with the barrier. 29
3.20 Density profile of the periodic 100x100 lattice with the barrier. 30
3.21 Density profile of the periodic 200x200 lattice with the barrier. 30
3.22 Density profiles of the open 100x100 lattice close to the coexistence line. 31
3.23 Density profiles of the open 200x200 lattice close to the coexistence line. 32

4.1 Fragment of the lattice with horizontally extended particles. 34
4.2 Row of the vacancies that cover the sites in question. 36
4.3 Possible jumps of the horizontally extended particle. 36
4.4 Fragment of the lattice with vertically extended particles. 38
4.5 Dependency of the current on the density in the 50x50 system with horizontally extended particles. 39

4.6 Dependency of the current on the density in the 100x100 system with horizontally extended particles. 39
4.7 Dependency of the current on the density in the 200x200 system with horizontally extended particles. 40
4.8 Phase diagram for the 50x50 system with horizontally extended particles. 41
4.9 Phase diagram for the 100x100 system with horizontally extended particles. 41
4.10 Phase diagram for the 200x200 system with horizontally extended particles. 42
4.11 Dependency of the current on the density in the 50x50 system with vertically extended particles. 43
4.12 Dependency of the current on the density in the 100x100 system with vertically extended particles. 43
4.13 Dependency of the current on the density in the 200x200 system with vertically extended particles. 44
4.14 Phase diagram for the 50x50 system with vertically extended particles. 45
4.15 Phase diagram for the 100x100 system with vertically extended particles. 45
4.16 Phase diagram for the 200x200 system with vertically extended particles. 46

5.1 Relationship $j_x(\rho)$ for the 50x50 ASEP model with vertical bias of particles. Probability to jump upward-right is $p = 0.3$. 52
5.2 Relationship $j_y(\rho)$ for the 50x50 ASEP model with vertical bias of particles. Probability to jump upward-right is $p = 0.3$. 52
5.3 Current ratio vs density of the particles in the 50x50 ASEP model with vertical particle drift. 53
5.4 Relationship $j_x(\rho)$ for the 100x100 ASEP model with vertical bias of particles. Probability to jump upward-right is $p = 0.3$. 54
5.5 Relationship $j_y(\rho)$ for the 100x100 ASEP model with vertical bias of particles. Probability to jump upward-right is $p = 0.3$. 54
5.6 Current ratio vs density of the particles in the 100x100 ASEP model with vertical particle drift. 55
5.7 Relationship $j_x(\rho)$ for the 200x200 ASEP model with vertical bias of particles. Probability to jump upward-right is $p = 0.3$. 56
5.8 Relationship $j_y(\rho)$ for the 200x200 ASEP model with vertical bias of particles. Probability to jump upward-right is $p = 0.3$. 56
5.9 Current ratio vs density of the particles in the 200x200 ASEP model with vertical particle drift. 57

6.1 Snapshot of the lattice with obstacle. 61
6.2 Density profiles in the 50x50 lattice with an obstacle. 62
6.3 Density profiles in the 100x100 lattice with an obstacle. 62
6.4 Density profiles in the 200x200 lattice with an obstacle. 63

List of Files

goykolov_thesis.pdf (2.2 MB)

Chapter 1

Introduction

The asymmetric simple exclusion process (ASEP) is the simplest case of the more common class of models known as driven lattice gases. Driven lattice gas models were introduced to study the effect of an external electric field on the ordering processes. In these models the particles are located on a lattice and their motion is affected by the interactions with neighbors and *an external field*. In the ASEP model the external field is represented by the asymmetry of the motion of particles.

Driven lattice gas models are stochastic lattice models with particles jumping preferentially in one direction. The stochastic models are convenient for the description of systems of interacting and hopping particles. In stochastic lattice gas models, the particles jump to neighboring sites but then lose memory of their past (direction of the jump, hopping probability etc.): successive jumps are independent. Hard core repulsion between particles is expressed by forbidding double occupation of a site. Unless reactions are involved or the system is open, the number of particles is conserved. Since direct analytic treatments are intractable, convenient approximations are necessary such as mean field theory (MFT). MFT assumptions that we will use will be explained below during the discussion of our models.

In most cases the left and right boundaries of the ASEP lattice are attached to particle reservoirs of constant densities which drive a stationary particle current in the steady state. But also we will consider closed systems with fixed number of particles. In this case the lattice is periodic along the horizontal direction.

The one-dimensional ASEP model was introduced in 1968 to understand protein synthesis by means of the one-dimensional motion of ribosomes along the RNA molecule [1]. The one dimensional model also can be applied to describe conductivity in zeolites [2]. Zeolites are minerals that have a micro-porous structure. Typical structure of a zeolite is shown on the Fig. 1.1.

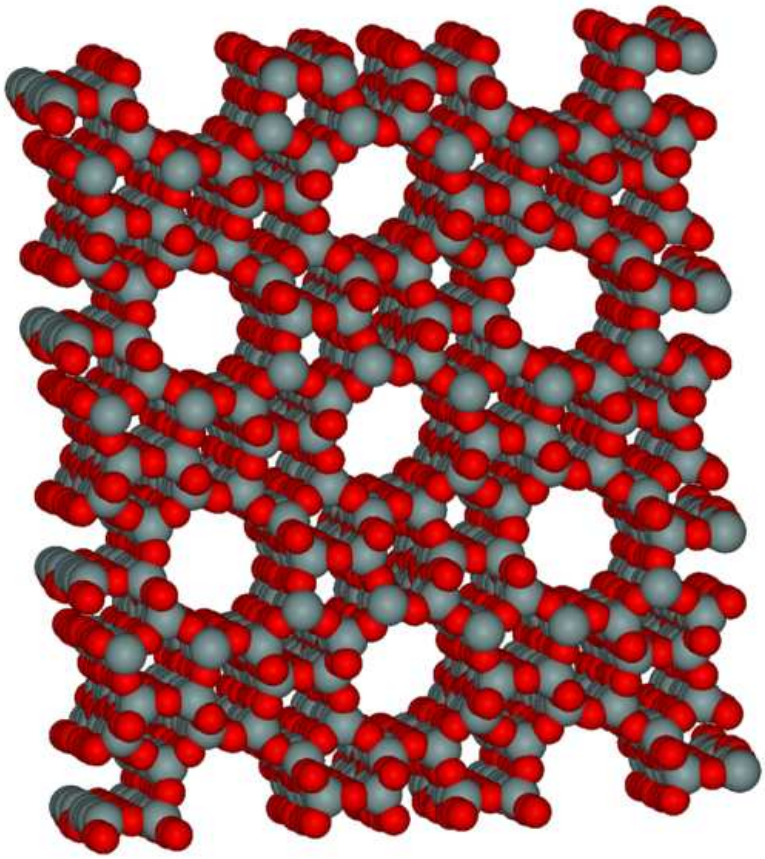

Figure 1.1: Structure of ZSM-5 zeolite.

Conductivity and diffusion in these materials occur along the one-dimensional channels in the crystal.

A generalization of the ASEP model has been applied to traffic flow problems [3], where each particle is associated with a car on an one-lane road (or a speedway between two junctions where cars may enter or leave the road). Other applications of the ASEP include growth models [4] and vortex models [5].

Polymer dynamics [6] can be mapped to the ASEP with open boundaries when considering hopping of the entangled polymer center of mass along the sequence of pores.

Protein synthesis [7] is described by means of the ASEP model with extended particles. The mechanism consists of ribosomes moving along an mRNA chain. Known as "translation", this process is often described as having three steps: initiation, where ribosomes attach themselves, one at a time, at the "start" end of the mRNA; elongation, where the ribosomes move down the chain in a series of steps; and termination, where they detach at the "stop" end of the molecule. Since ribosomes cannot overlap, their dynamics is subject to the "excluded volume constraint".

Gel electrophoresis [8] of DNA also may be described as ASEP model. In this model a chain of charged DNA bases (called "reptons" in this literature) moves in the vertical axis along separate one-dimensional channels, with the hopping condition dictated by the configuration of neighbor reptons.

In one dimension, the ASEP model has been widely studied, and exact solutions have been found using the infinite dimension matrix method [9]. Other main application of the 1D model are given above. However, to our knowledge, very little is known concerning the 2D ASEP model. Applications of the 2D model can be found in such contexts as granular sheared flow, pipe flow, pyroclastic flows [10]. The granular flow model describes the flow of particles that move along a system of parallel rows. The hopping probability depends on the nearest neighbor configuration of the particles, not only on the row where the particle is located, but also depending on the configuration of particles on neighboring rows. However, no transitions from one row to another are allowed. Pyroclastic flows are a common result of some volcanic eruptions. It is a flow of fluidized masses of rock fragments and gases that move rapidly in response to gravity.

The traffic flow models [11, 12] employ two-dimensional features only in one case. The motion of vehicles is modeled as a hopping of particles along one-dimensional lattice. But if the site in front of the particle is occupied it may undertake so called

jam-avoiding turn (either changing direction of motion from, for example, going to the right to going up or changing lanes by hopping to the neighbor row).

Paper [13] describes two models of two-dimensional traffic flow. Both have a square lattice filled with cars and no more than one car can be present at any site. In the first model half of the cars move preferentially to the right (with some small probability to jump in the vertical direction) and other half of the cars is moving preferentially upward (with a small probability to jump to the right). The second model is defined in such a way that it has streets (rows and columns of the lattice) that point alternatively up and down, and right and left (set of one-way streets).

Another two-dimensional approach to the traffic flow model [14] used two-lane traffic with cars moving in opposite direction. Each lane represented one-dimensional ASEP model. Hopping probability of the particle (velocity of the car) reduced if another car approached on the other lane.

A similar model is used to describe bi-directional motion of ants [15]. In this model ants are moving along two channels (trails), and the probability to jump (move) forward changes if another ant is approaching on the other trail.

Kolomeisky [16] has studied a model which consist of two parallel one-dimensional channels with particles moving along them. A particle at site i can hop up (or down) to the same site i on the other channel with rate $0 \leq w \leq 1$, if that site is empty. The particle can also move from left to right along the same channel to site $i+1$, if this site is not occupied. However, this transition rate depends on occupation of site i at the neighboring channel. If there is no particle at that site, the rate is equal to $1-w$, otherwise the particle jumps with the rate 1.

The simplicity of the model has made it the default stochastic model for transport phenomena. Furthermore, it is also a basic component for models [17] with incompressible Navier-Stokes equations as the hydrodynamical equation. In this model ASEP is slightly modified. Each particle in the flow model is assigned a certain velocity. Particles still move on a lattice, jumping in one preferred direction. The modification of the model allows two particles with different velocities to occupy one lattice site. This process is called collision, after which (when those two particles leave the site) the particles that have collided have new velocities.

Shock fluctuations in the two-dimensional ASEP model were studied [18]. In this model particles were situated on a square lattice and were allowed to jump in

four different directions (up, down, right or left). Asymmetry was implemented by making the probabilities to jump right and left different. Probabilities to jump up and down though remained equal.

The ASEP model has been applied to computer network traffic [19, 20]. In a one-dimensional model a chain of sites (routers) is used with finite capacity for data packets (particles), meaning that only several particles can occupy one lattice site. Particles are created at the source and terminated at the destination point. The goal of the problem is to deliver the particle from the source to the destination within the shortest period of time. A two-dimensional version has also been described, in which particles travel on a square lattice of nodes (sites). When a particle (data packet) has a choice of more than one node to jump to, the probability of the jump to a particular node is calculated. These probabilities are not equal to each other, thus providing asymmetry in the motion of the particles.

Pedestrian dynamics can be studied by means of a 2D ASEP [21, 22]. An LxW lattice is populated with particles that are allowed to occupy only one lattice site and move preferentially to the right. The lattice is periodic in the horizontal direction and has impenetrable walls on the top and bottom boundaries. In this model shuffle update algorithm was used. The general practice for the ASEP models is to use sequential updates, where at any given time step any particle may be chosen and tested for the jump. In the shuffled update scheme the update procedure also starts from the random choice of a particle. But after that this particle doesn't take part in the draw, meaning that we can choose any remaining particle except those which were already chosen. When all particles on the lattice were chosen the process starts over.

The two-species asymmetric diffusive process [23] is modeled on the two-dimensional lattice with two types of particles. The first set of particles is allowed to move only along the positive x direction (to the right) and second set of particles moves to the positive y direction. Particles obey hard-core exclusion interaction and can not change direction of hopping (from vertical to horizontal or vice versa).

The two-dimensional ASEP model has been extended to the nearest-neighbor exclusion interaction of particles [24]. In this model particles are jumping on the two-dimensional square lattice. The probability to jump up/down is the same, i.e. there is no asymmetry in vertical direction. But the preferred direction of the jump

in horizontal direction is to the right. Particles interact through nearest-neighbor exclusion principle. This means that the distance between any pair of particles must be larger than one lattice spacing. This is the closest problem to those that will be described in this work. The goal of this paper was to study the phase transitions between low density and high density (jammed) states.

The asymmetric exclusion model (both one- and two-dimensional) has attracted attention in mathematics, particularly in probability theory [25, 26, 27].

The papers that deal with the two-dimensional features of the ASEP model reviewed here study various aspects of it, but none of them treat the problems that are discussed in this thesis.

The purpose of this work is to present results of the following models. First we study the simplest ASEP model which possesses particle-hole, transverse, and translational symmetries using a model of a square lattice with particles that occupy one lattice site and move to the right along the diagonals of the squares. It appears that in many respects the results of this model coincide with those of a one dimensional model. We also find good agreement between mean-field theory and simulations except close to a domain wall – the boundary between separated phases.

We then study the consequences of relaxing the various symmetries. We can break the particle-hole symmetry by modifying the model so that the particles occupy more than one lattice site. We will present results for the current flow, density distribution, and the phase diagram, as obtained by Monte-Carlo simulations and mean-field theory.

Transverse symmetry can be removed by allowing the jumps in different directions to have different probabilities. This usually will lead to a transverse drift of the particles. Mean-field theory will be used to determine the longitudinal and transverse currents for this case; these will be compared with the Monte-Carlo simulations.

Also we explore the system with an immovable obstacle. An obstacle is one or several particles located at fixed position. In this model we observe an increase in particle density in front of the obstacle and a "shadow" behind it. It is expected that the shape and size of those formations are symmetrical in transverse direction.

Chapter 2

Definition of the Models

2.1 One Dimensional Model.

2.1.1 Definition of the Model.

This section introduces the ASEP model and summarizes the main results for the one-dimensional case.

The ASEP is a stochastic lattice model for particles that jump preferentially in one direction: the jump probability is asymmetric. The particles interact by a hard core exclusion rule (Fig. 2.1), so that no more than one particle is allowed to occupy a lattice site. The only version we will consider is the totally asymmetric process, for which particles can only move in the positive direction (to the right).

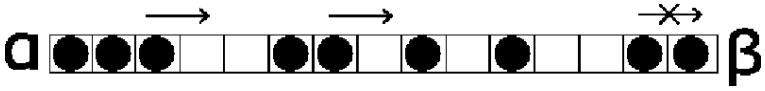

Figure 2.1: One-dimensional ASEP model.

In the bulk at each time step a particle will move from site x to site $x+1$ if the target site is vacant. The first and the last sites of the system are connected to reservoirs of particles that try to impose a particle density within it. At the left end the reservoir supplies particles; if the first site in the lattice is empty a particle enters with probability α in each time step. This would give a steady state if the density in the bulk were also α. At the right end particles are removed with probability β, which would give steady state if the density were $1-\beta$. Thus for general α and β we are trying to impose a gradient in particle density.

The system was studied by means of the Monte Carlo method with sequential lattice update. At every moment of time one lattice site is chosen. If it is on the left edge and is empty it can be populated with probability α. If the chosen site is at the right edge and is occupied with a particle, it is extracted with probability β. If the site is in the bulk of the lattice and contains a particle, it is tested for the jump to the neighbor site. The particle does jump if the neighboring site is vacant.

The one-dimensional system has been widely studied [28, 29] (and references therein). Here we just present main results for this model.

2.1.2 Phase Diagram for the One Dimensional Model.

The one-dimensional model has hole-particle symmetry: in the high density phase the motion of particles to the right is equivalent to the motion of vacancies in the low density phase to the left. It follows that the current density for a system with a low density ρ is the same as the current density for a system with a high density $1-\rho$, suggesting that as a function of ρ the current density j will have a maximum at $\rho = \frac{1}{2}$. According to mean-field theory, the functional form is $j = \rho(1-\rho)$, as will be shown below. When the boundary conditions are trying to impose differing densities at the edges, the "phase" with the lower current density will tend to expand and dominate the system. This occurs because the current is controlled by the entrance or exit rates. If α is sufficiently small, the current in the lattice depends on it. It is limiting the entrance of new particles into the system. On the other hand, if β is small enough so it is limiting the exit rate of the particles, the exit rate will control the current in the system for a wide range of values for α. Thus for $\beta \leq \frac{1}{2}$ and $\beta < \alpha$, the system is filled with a high density phase, with current $\beta(1-\beta)$ and bulk density equal to $1-\beta$ almost everywhere except near the left boundary. In this case extraction of the particles at the right edge is the limiting process. For $\alpha \leq \frac{1}{2}$ and $\beta > \alpha$ there is a low density phase with current $\alpha(1-\alpha)$. In this phase the bulk density equals α. The limiting process here is the rate of particle supply. At the co-existence line $\alpha = \beta < \frac{1}{2}$, the two phases have the same current density and can coexist, separated by a domain wall (a region where there is a rapid step-like change in the density of the particles). Finally, a phase of maximal current exists in the region $\alpha \geq \frac{1}{2}$ and $\beta \geq \frac{1}{2}$: the density equals approximately $\frac{1}{2}$ and smoothly changing from α on the left edge to $1-\beta$ on the right edge, and the current is close to the maximal value $\frac{1}{4}$.

Below is the resulting phase diagram for the one-dimensional model. The high and low density "phases" meet with a discontinuous "phase transition" at the solid line: as $\alpha - \beta$ changes sign, the domain wall moves from one edge of the system to the other. The boundary to the "maximal current" region is more subtle: the

length scale on which the density varies becomes infinite along the dashed lines, and is infinite throughout the "maximal current" phase.

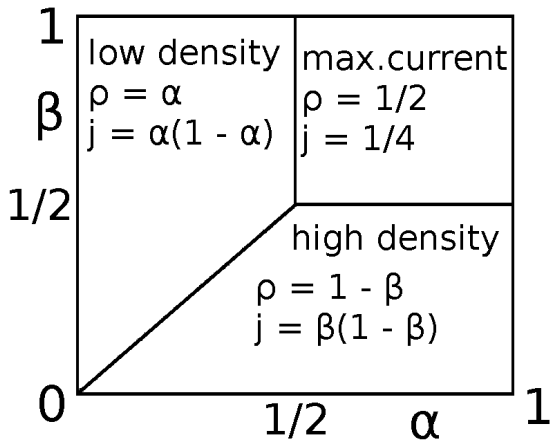

Figure 2.2: Phase diagram for the one dimensional ASEP model.

In the infinitely long lattice, the hard core exclusion rule of interaction implies that the steady state particle current j is related to the bulk density ρ by [30]:

$$j = \rho(1 - \rho). \tag{2.1}$$

A graph of this dependency is shown below (Fig. 2.3).

For all α and β (except when $\alpha = 1 - \beta$) there will be a spatial variation in the density along the system [28]. Far from the co-existence line the bulk of this change takes place close to the boundaries. For example, in the high density phase the density will change from α to $1 - \beta$ near the left edge. If the system is in the low density phase this change happens close to the right edge and changes from the bulk density α to the right edge density $1 - \beta$. At the co-existence line (and close to it), the transition in density from α to $1 - \beta$ occurs in the bulk of the system. The region where this fast step-like change in density takes place is a domain wall between the low and high density regions of the lattice.

As will be shown later, current in the system depends not only on the density, but also on the density gradient along the lattice. In the infinitely long lattices those gradients are extremely small and can be neglected. Therefore, the current is described by the Eq. (2.1). When the lattice is short density gradients bring sensible contribution to the current in the system. Below we will show that in this case the

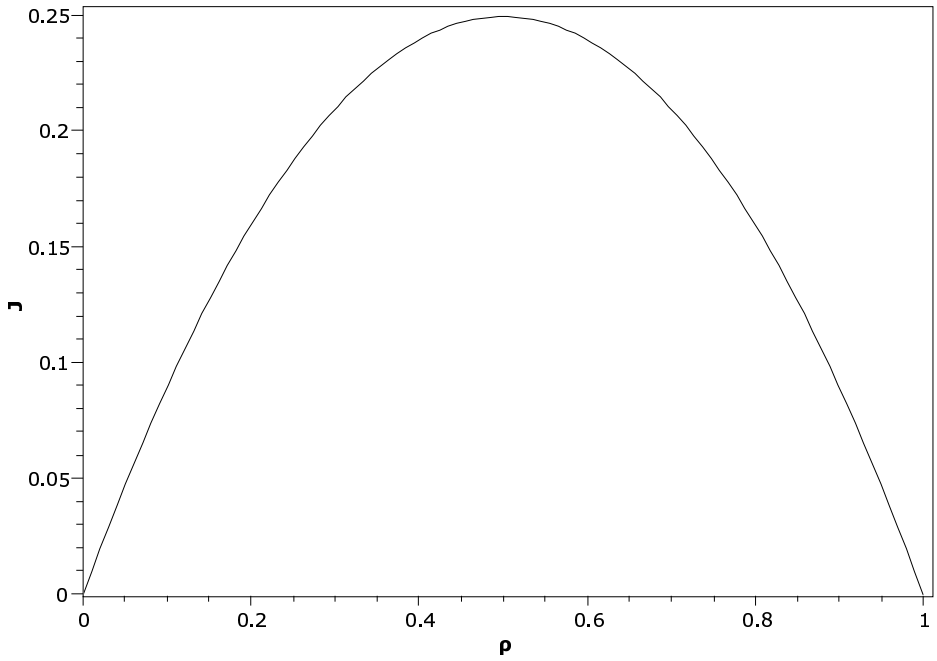

Figure 2.3: Dependency of the current on the bulk density of the particles in one-dimensional ASEP model.

density will slowly change along the system from α to $1-\beta$ and the current density can be (slightly) larger than $\frac{1}{4}$.

2.2 Two-Dimensional Model

We have extended the model to two dimensions. Now the particles occupy the sites of a square lattice (Fig. 2.4). The totally asymmetric model is considered, meaning that only jumps to the right are allowed. The particles continue to obey a hard core exclusion rule of interaction. They are allowed to jump only along the diagonals to the neighboring sites to the right provided that the site is not occupied. This confines a particle to one of the two sublattices (like on the chess board). This model was chosen in preference to allowing the additional move directly to the right to avoid introducing a new parameter, since there is no reason for the diagonal jumps and direct jumps to occur with the same probability.

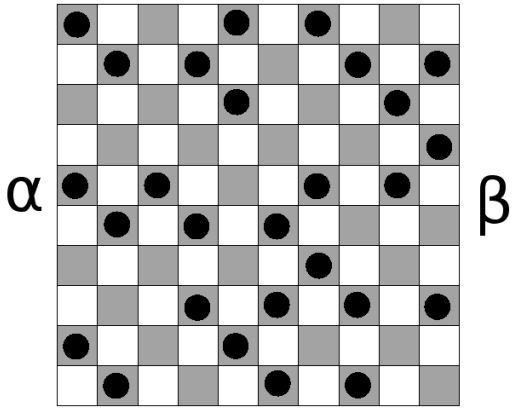

Figure 2.4: Two-dimensional ASEP model.

On the left edge, particles are supplied with the rate α if the chosen site on the left boundary is empty, and are removed on the right edge with the rate β if the chosen site on the right boundary is occupied by a particle. There are periodic boundary conditions on the top and bottom boundaries of the lattice. Since particles on the two sublattices cannot interact, we will only populate one of them (the sublattice on which sum of site indices is even number).

The coordinate system and labeling of the sites are shown on the Figure 2.5 below. We will keep this convention for all models in this text (unless stated otherwise).

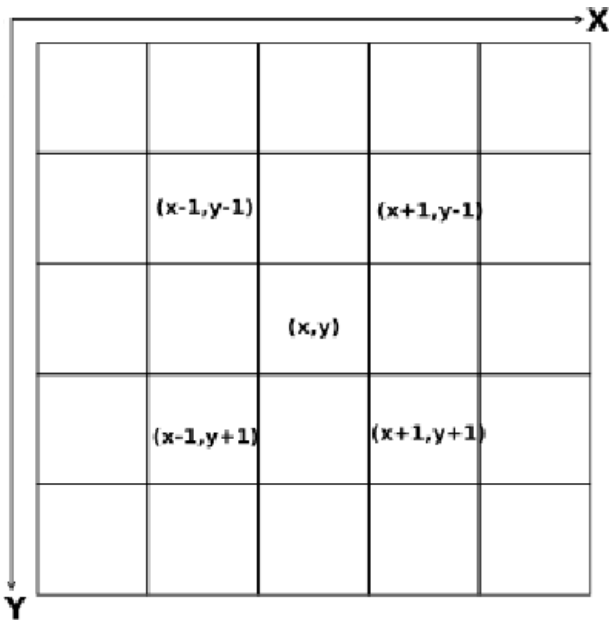

Figure 2.5: Coordinate system and labeling of the sites.

Chapter 3

Two-Dimensional Model

3.1 Mean-Field Theory for Regions Far From Critical.

In this chapter we consider the simplest two-dimensional model: particles that occupy only one lattice site, with equal probability of jumping along the two diagonals.

The mean-field approximation to this model assumes that the correlations between particles can be ignored:

$$< n(x,y)n(x',y') >=< n(x,y) >< n(x',y') >= \rho(x,y)\rho(x',y'). \qquad (3.1)$$

This assumption is appropriate for our system because the location of each particle is independent of the location of any other particle. In another words, knowing the density on the site (x, y) doesn't tell us anything about density at the site (x', y'). This means that we can replace the actual particle density (which is either zero or unity at every site) by the ensemble-averaged density ρ, which is a differentiable function of position; then the probability that a particle will move from a site $\vec{x}$ to a neighboring site $\vec{y}$ is just $\rho(\vec{x})(1 - \rho(\vec{y}))$.

The particle density at a site will change in time if there is an imbalance in the arrival and departure of particles. For the lattice site at (x, y), this gives

$$\frac{\partial \rho}{\partial t} = \frac{1}{2}(\rho(x-1, y+1)+\rho(x-1, y-1))(1-\rho(x, y))-\frac{1}{2}\rho(x, y)(1-\rho(x+1, y+1)+1-\rho(x+1, y-1)). \tag{3.2}$$

where the four terms describe the four processes that affect the occupancy of site (x, y); the factor of $\frac{1}{2}$ is the probability of choosing one of the two diagonals from a site.

We assume that the function of density slowly changes with x so that it can be expanded into a Taylor series. Keeping terms of first and second order in the gradients we obtain

$$\frac{\partial \rho}{\partial t} = -\rho_x + 2\rho\rho_x + \frac{1}{2}(\rho_{xx} + \rho_{yy}) \tag{3.3}$$

This is the mean-field equation for ρ. It can be written in the form of a continuity equation

$$\frac{\partial \rho}{\partial t} + \vec{\nabla} \cdot \vec{j} = 0 \tag{3.4}$$

where

$$\vec{j} = -\frac{1}{2}\vec{\nabla}\rho + \hat{x}(\rho - \rho^2). \tag{3.5}$$

which is the current density. The first term is the diffusive part of the current, which is driven by gradients; the second term is the drift current, which is a consequence of the spatial asymmetry of the process being considered.

In many cases the gradient of ρ is small and we can ignore the diffusive part. This can be done in a uniform system for $\alpha = 1 - \beta$, where there are no density gradients. In large systems the density gradient is negligibly small almost everywhere. This is the approximation that was used in the discussion above, that leads to

$$j = \rho(1 - \rho). \tag{3.6}$$

3.2 The Case of Transverse Symmetry and Steady State.

In the steady state there is no time dependence, so that $\dfrac{\partial \rho}{\partial t} = 0$. Eq. (3.3) becomes an elliptic partial differential equation for the dependence on x and y.

When there is no preferred jump direction along the vertical axis, there will be no

net current along this axis, and the particle density will not depend on the vertical coordinate y. We will first consider this case, and then take up the cases with more general spatial dependence subsequently.

With these assumptions, the density only depends on one coordinate, and the mean-field theory becomes the one-dimensional theory, allowing direct comparison between one and two dimensions. The continuity equation implies that the current density is independent of position, giving us a first integral

$$\frac{1}{2}\rho' = \rho - \rho^2 - j, \tag{3.7}$$

where j is the constant value of the current density. This equation is readily solved. There are two cases. When $j \leq \frac{1}{4}$, we have the solution

$$\rho(x) = \frac{1}{2} + \frac{1}{2}\sqrt{1-4j}tanh[(2x-2C)\sqrt{1-4j}], \tag{3.8}$$

where C is a constant of integration. This solution is nearly constant except for x near C, where there is a well-localized transition from a low density to a higher one: a domain wall. We note that ρ is monotonic increasing. This describes the density profile for the high- and low-density phases, including the coexistence region if there is one.

This solution indicates that there is a characteristic length

$$\xi = \frac{1}{\sqrt{1-4j}}. \tag{3.9}$$

which makes sense when $j < \frac{1}{4}$. It characterizes the width of the domain wall between the high and low density phases.When one of these phases is present and has a density ρ_∞ well away from the wall, we can substitute $j = \rho_\infty(1-\rho_\infty)$ to get

$$\xi = \frac{1}{1-2\rho_\infty} \tag{3.10}$$

A similar length scale results from linearizing Eq. (3.5) with the assumptions that ρ and j are nearly constant. Note that these considerations identify the maximum of Eq. (3.6) (and more generally, the maximum current that can be carried by a uniform system) and the corresponding density as being critical cases, where the

length scale diverges. We have derived our theory by assuming that the correlations between particles are short ranged. Close to the critical current, however, they may become longer ranged, and have a different dependence on system parameters than given here. This would parallel the situation for the critical points in thermodynamic systems.

The other case is for $j \gtrsim \frac{1}{4}$. Since the drift current cannot exceed $\frac{1}{4}$, this requires a contribution from the diffusive current, implying $\rho' < 0$. The solution in this case is [33]:

$$\rho(x) = \frac{1}{2} - \frac{1}{2}\sqrt{4j-1}tan[(x-C)\sqrt{4j-1}]. \tag{3.11}$$

The divergences of the tangent function must occur beyond the boundaries of the system; within the physical range, ρ is close to $\frac{1}{2}$ with a small negative gradient of order $2j - \frac{1}{2}$. This solution describes the "maximal current" phase. We observe that in this phase we do not have an exponential function localizing variations in the density; there isn't a characteristic length apart from the system size itself.

3.3 Simulation Results and Comparison with the MFT.

In this section we present the results of the Monte Carlo simulations for the two-dimensional model described above (particles that occupy a single site on the square lattice), and compare them with the predictions of the mean-field theory.

The simulations used a Monte Carlo algorithm with sequential update. At each time step a site is chosen at random. If it is on the left edge of the lattice and it is empty, then the site will become occupied with probability α. If the chosen site is on the right edge and it is occupied, then the particle can be extracted from the system with the probability β. If the site is in the bulk of the lattice and is occupied by a particle then one of the two possible neighboring sites is chosen (again at random, and for this model they are chosen with equal probability), and the particle is moved to this target site if it is empty.

Occasionally it was useful to study a closed system, in which the number of particles is fixed. This was done by connecting the right and left edges of the system, so that a particle leaving at the right immediately reentered at the left. The two boundary conditions collapse into one: a probability γ that a particle at the right edge will hop into an empty site at the left edge. The case $\gamma = 1$ is the completely

periodic system.

Density at the right half and at the left half of the lattice are related. For example, if the density at the left edge is ρ, then density at the right edge is $1-\rho$. Since the system is in the steady state, the current is constant and uniform along the lattice and it depends on the particle jump probability in the bulk of the system, which is equal to $\rho(1-\rho)$. The same probability holds for the jump of the particle from the right edge to the left edge. The probability that the site at the right edge is occupied is equal to $1-\rho$. The site at the left edge will be empty with the probability $1-\rho$. And the probability of the jump will be equal to the product of these two probabilities and the barrier factor γ. Besides, jump probability in the bulk should be equal to the jump probability at the edges. This gives:

$$\rho(1-\rho) = \gamma(1-\rho)(1-\rho). \tag{3.12}$$

After solving this equation for the density we have:

$$\rho = \frac{\gamma}{1+\gamma}. \tag{3.13}$$

For our case of $\gamma = 0.3$ the density at the left half of the lattice is $\rho \approx 0.23$.

When the system has open boundaries we can start the simulation with an arbitrary initial density. After the system reaches steady state it will have the density dictated by the boundary conditions. The initial density in our simulations was chosen to be 0.25. Simulations were done for three lattices of different size - 50x50, 100 x 100 and 200x200 sites. For 50x50 and 100x100 lattices the time of one run was 10^5 MC steps and for 200x200 sample it was 5×10^4, which allowed the system to reach the steady state and to collect enough statistics.

Since we expect the density to be independent of the transverse coordinate y, the particle occupation numbers were combined for each column to determine $\rho(x)$. To test this assumption we performed 3 independent runs on the closed 100x100 lattice model. The density of the particles in the system was set to be 0.5, $\gamma = 0.3$. The density was normalized so that $\rho = 1$ means all available sites in a column are occupied.

For these three runs average values of the density along the vertical axis are:

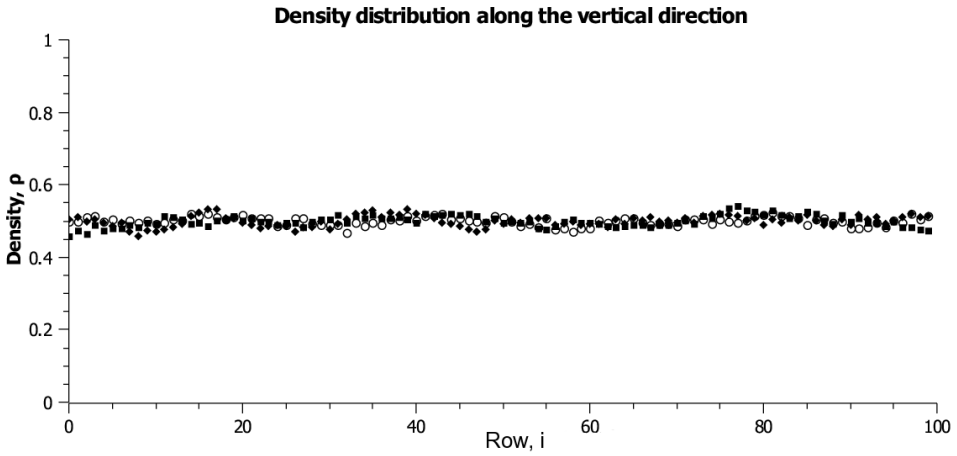

Figure 3.1: Density distribution along the y axis in the periodic 100x100 lattice.

0.5 ± 0.016, 0.5 ± 0.015 and 0.5 ± 0.012. Average value of the vertical density is equal to the initial density of the particles in the lattice and doesn't depend on the change of the position along y axis.

Next we will present sets of graphs showing the results of MC simulations (performed on the open system) for three different samples and compare numerical and MFT results.

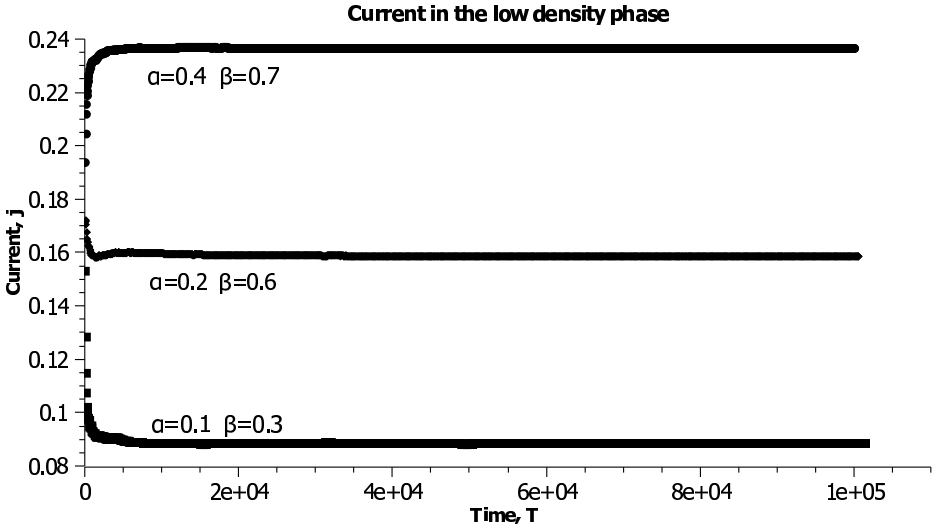

Figure 3.2: Average current vs time in the 50x50 system with dominating low density phase.

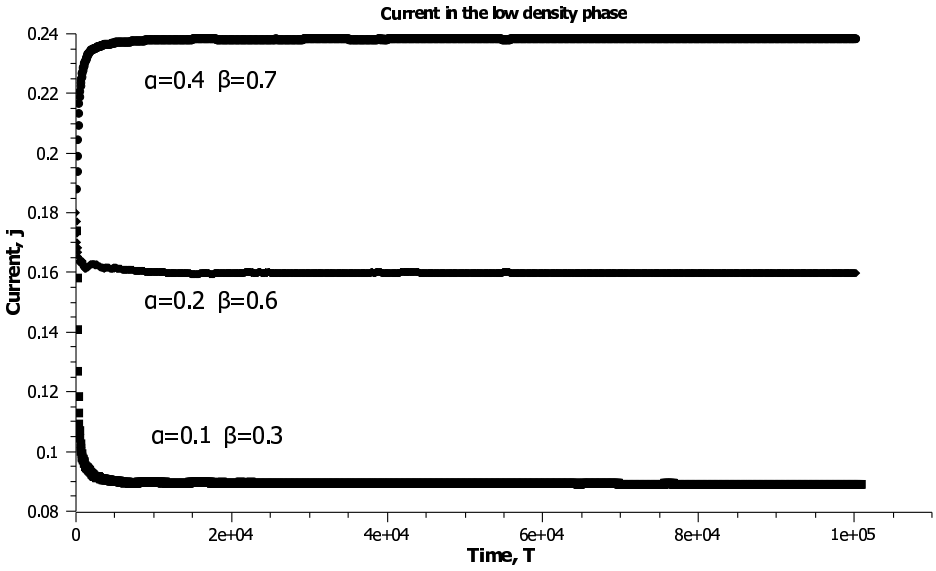

Figure 3.3: Average current vs time in the 100x100 system with dominating low density phase.

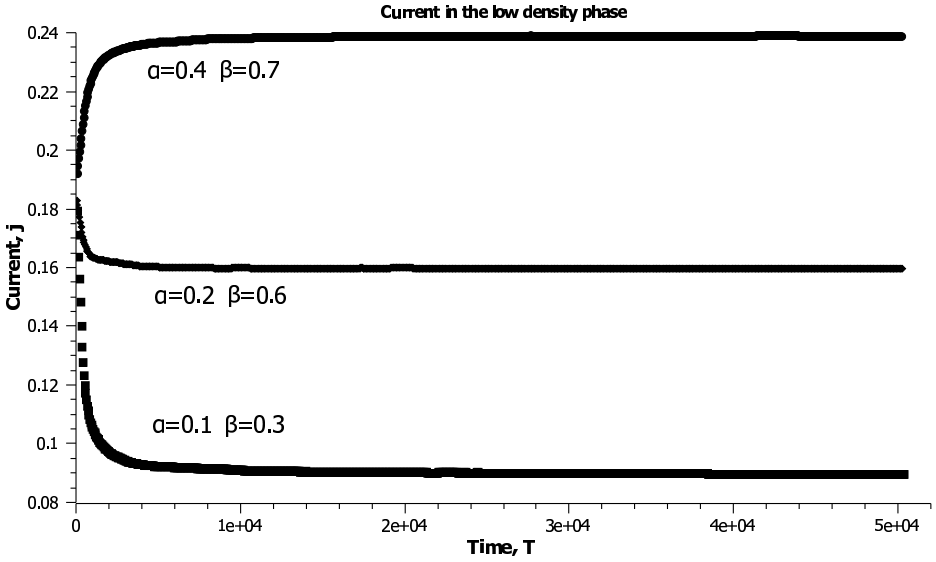

Figure 3.4: Average current vs time in the 200x200 system with dominating low density phase.

Figures 3.2, 3.3 and 3.4 show how the average current depends on the averaging time. Since in all simulations we start with the fixed initial density 0.25 all graphs start from approximately the same value of current. The system quickly attains

steady state. Independent of the size of the lattice all three graphs show the same behavior of the average value of the current. Starting from some value that was dictated by the initial density of the lattice three curves quickly go to the steady-state values of the current.

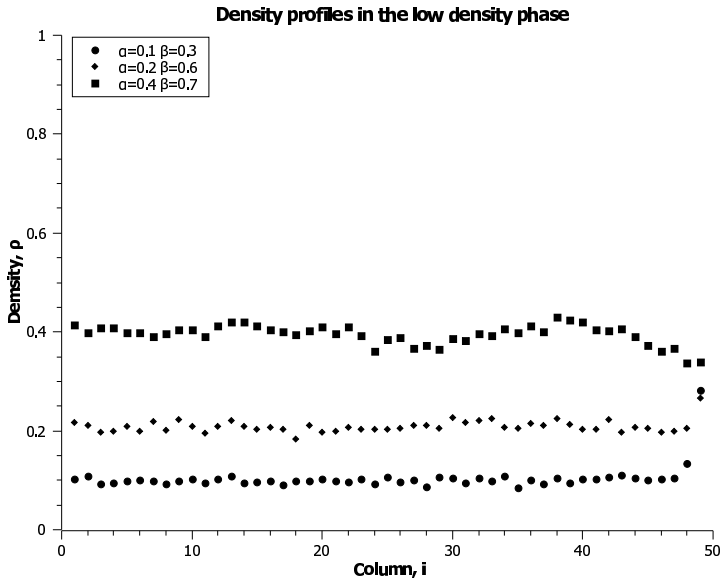

Figure 3.5: Density profiles in the 50x50 system with dominating low density phase

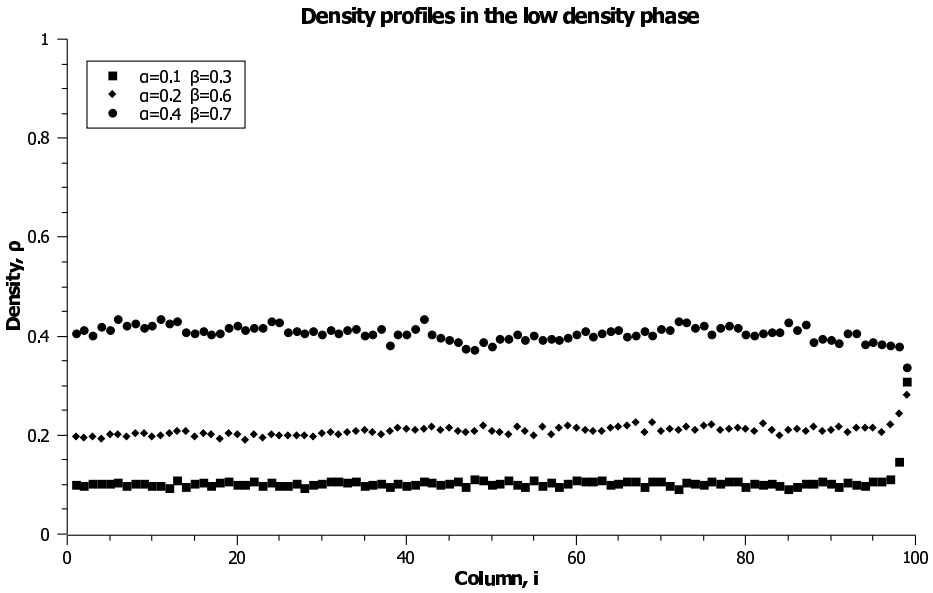

Figure 3.6: Density profiles in the 100x100 system with dominating low density phase

Figures 3.5, 3.6 and 3.7 show the density profiles in the systems for the same

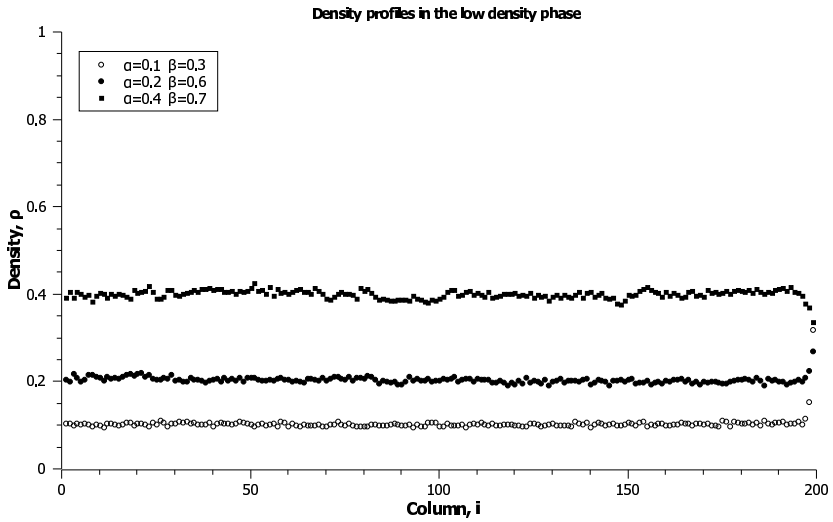

Figure 3.7: Density profiles in the 200x200 system with dominating low density phase

boundary conditions as graphs of the current . Density was measured when the system had already reached the steady state. Since the system is in the low density state, the limiting parameter is α and the bulk density of the particles is equal to α. On the right side of the lattice we can observe that the density of the particles tends toward $1-\beta$. Graphs for all three lattice sizes obey described above behavior. And as one can see with increasing the size of the lattice the behavior of the curve doesn't change.

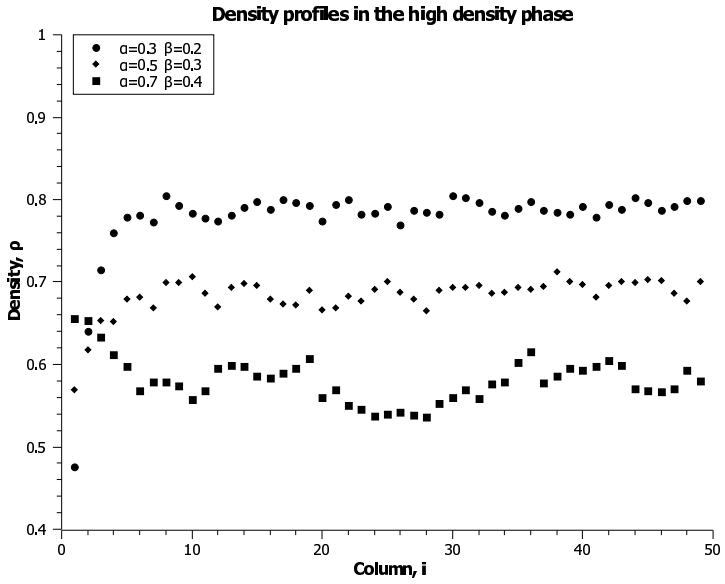

Figure 3.8: Density profiles in the 50x50 system with dominating high density phase

These two sets of graphs are consistent with the mean-field theory for the density and current in the lattice. To show that we give one particular numerical result. For example, for $\alpha = 0.2, \beta = 0.6$ we have $\rho = \alpha = 0.2$ and $j = \rho(1-\rho) = \alpha(1-\alpha) = 0.16$. Further we need to consider each lattice to take into account diffusive terms:

- in 50x50 lattice, $\rho' \approx \dfrac{\Delta\rho}{\Delta x} \approx 0.008$, therefore, $j \approx 0.156$. From the simulation we get, that $j_{sim} \approx 0.1588 \pm 0.00071$ and density of the particles is $\rho_{sim} \approx 0.2 \pm 0.0121$;

- in 100x100 lattice, $\rho' \approx 0.004$ and $j \approx 0.158$. Simulation results are $j_{sim} \approx 0.159 \pm 0.0099$ and $\rho_{sim} \approx 0.21 \pm 0.01126$;

- for 200x200 lattice $\rho' \approx 0.002$ which gives $j \approx 0.159$. From the simulations result one can see that $j_{sim} \approx 0.16 \pm 0.0017$ and $\rho_{sim} \approx 0.204 \pm 0.00741$.

Next we show graphs with density profiles for the high-density phase (Fig. 3.8, 3.9 and 3.10).

In the high density phase, the controlling parameter is β. The density in the bulk and on the right edge is equal to $1 - \beta$. On the left edge the density approaches α.

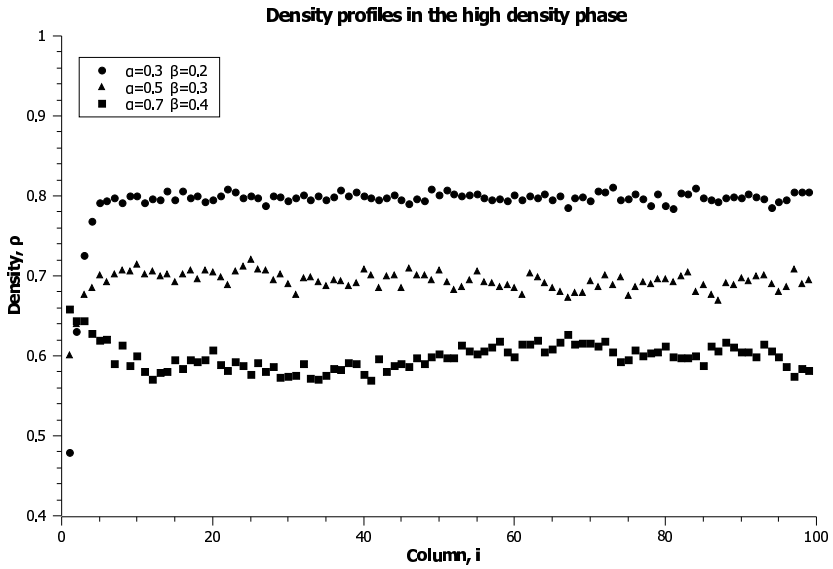

Figure 3.9: Density profiles in the 100x100 system with dominating high density phase

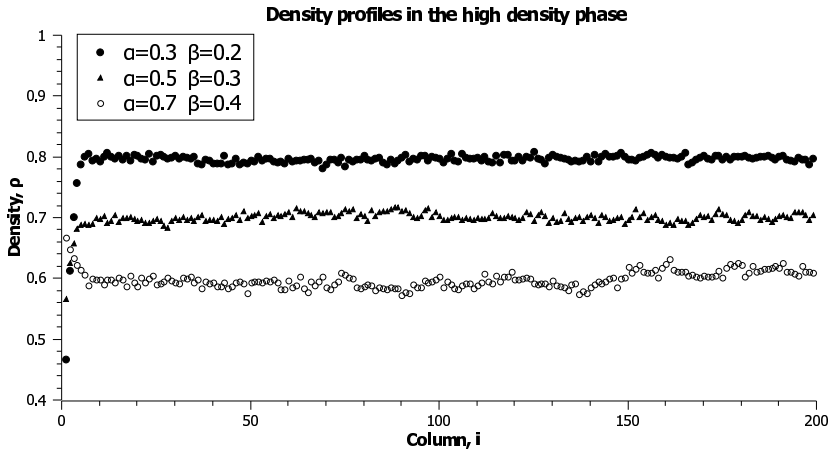

Figure 3.10: Density profiles in the 200x200 system with dominating high density phase

Here we also see consistency with the MFT calculations. For example, for $\alpha = 0.3, \beta = 0.2$: the density in the system is $\rho = 1 - \beta = 0.8$ and for the current we have $j = \rho(1-\rho) = \beta(1-\beta) = 0.16$. For three tested lattices we have:

- for 50x50 lattice, $\rho' \approx 0.01$ and $j \approx 0.155$. From the simulations we have $j_{sim} \approx 0.158 \pm 0.00234$ and $\rho_{sim} \approx 0.78 \pm 0.05079$;
- for 100x100 lattice, $\rho' \approx 0.005$, from which we have $j \approx 0.1575$. From the simulations we have got $j_{sim} \approx 0.16 \pm 0.00386$ and density $\rho_{sim} \approx 0.79 \pm 0.03722$;
- for 200x200 lattice the density gradient is $\rho' \approx 0.0025$, consequently, $j \approx 0.15875$. Simulations give us $j_{sim} \approx 0.164 \pm 0.006904$ and $\rho_{sim} \approx 0.79 \pm 0.02808$.

For the maximal current phase graphs with only one data set is presented ($\alpha = \beta = 0.6$) because other values for these parameters give very similar results (Fig. 3.11, 3.12, 3.13). The density on these graphs slowly varies from α to $1 - \beta$ on the edges. This agrees with the mean field theory, which predicts a nearly constant gradient for ρ. Also on these graphs we show the density distribution given by the MFT and Eq. (3.11) for the system where density gradient is less then zero.

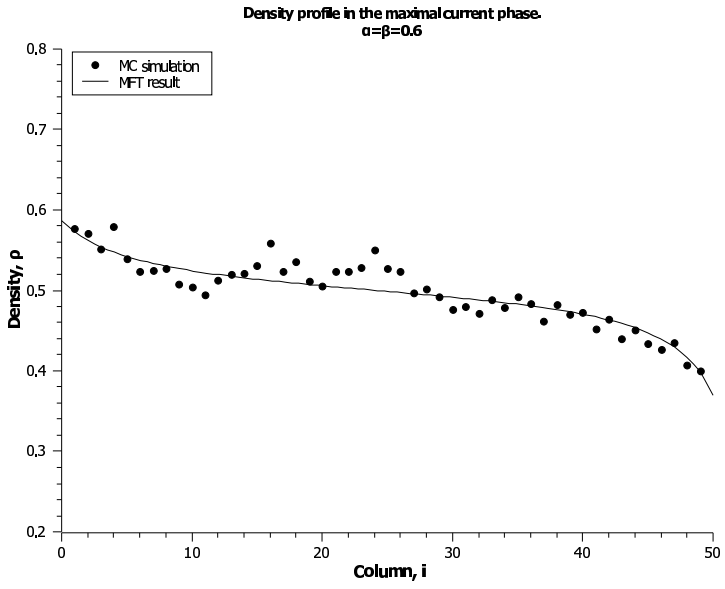

Figure 3.11: Density profile for the maximal current phase in 50x50 lattice.

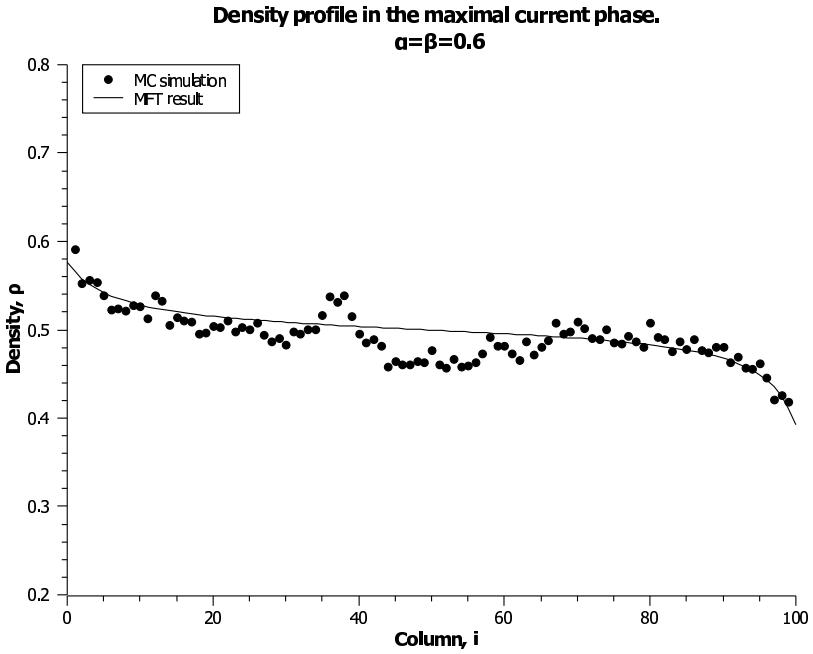

Figure 3.12: Density profile for the maximal current phase in 100x100 lattice.

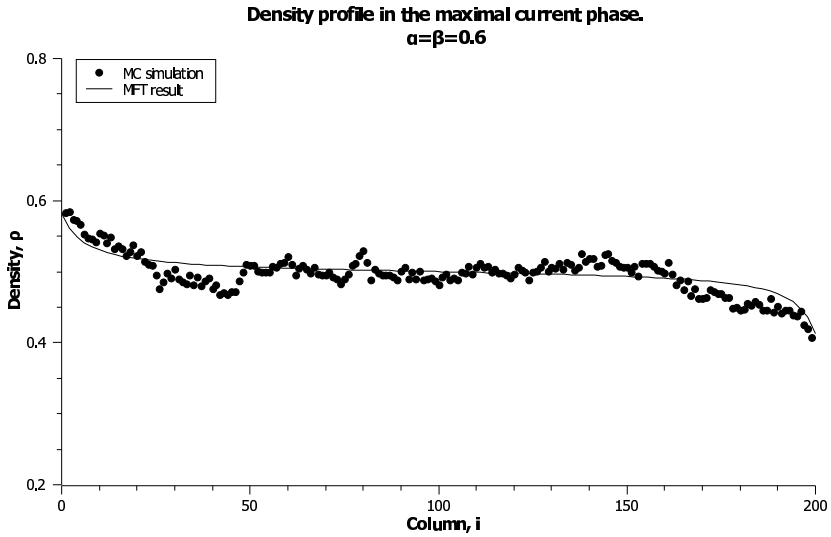

Figure 3.13: Density profile for the maximal current phase in 200x200 lattice.

The comparison of the results for these particular lattices are following:

- for 50x50 lattice $\rho' \approx -0.004$, hence, $j \approx 0.252$. From the simulation we have $j_{sim} \approx 0.247 \pm 0.0013$ and the density of the particles is $\rho_{sim} \approx 0.5 \pm 0.04218$, whereas MFT value of the density in the maximal current phase is 0.5 and current should be equal to 0.25;

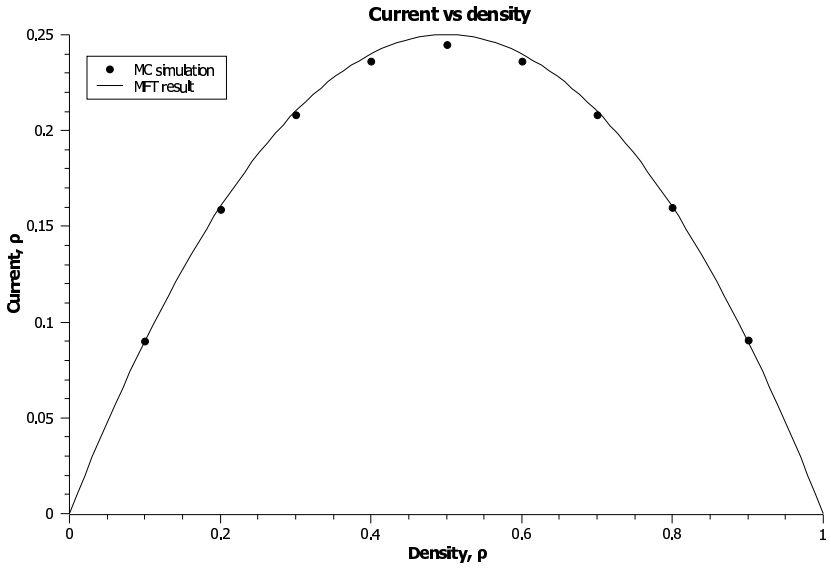

Figure 3.14: Current vs density plot for the 50x50 lattice.

- for 100x100 system, $\rho' \approx -0.002$. This means that $j \approx 0.251$. Simulation result is $j_{sim} \approx 0.248 \pm 0.00258$ and density is $\rho_{sim} 0.49 \pm 0.02877$;
- for 200x200 lattice, $\rho' \approx -0.001$, and $j \approx 0.2505$. But from the simulation we got $j_{sim} \approx 0.247 \pm 0.00524$ and the result for density is $\rho_{sim} \approx 0.5 \pm 0.02827$.

Comparing results of the simulation and MFT results we can assert that the size of the systen has effect on the density gradient and, therefore, on the deviation of the simulation result from the MFT values. With our choice of boundary conditions, the density gradient is approximately equal to $\frac{(1-\beta)-\alpha}{L}$. Hence, the larger the system (L), the smaller the gradient is and the closer the simulation result to the MFT result.

Figures 3.14, 3.15 and 3.16 show how the current depends on the density, according to mean-field theory and the MC simulations (performed on the open system). The MFT result is Eq. (3.6). As we can see experimental data resembles MFT curve fairly well.

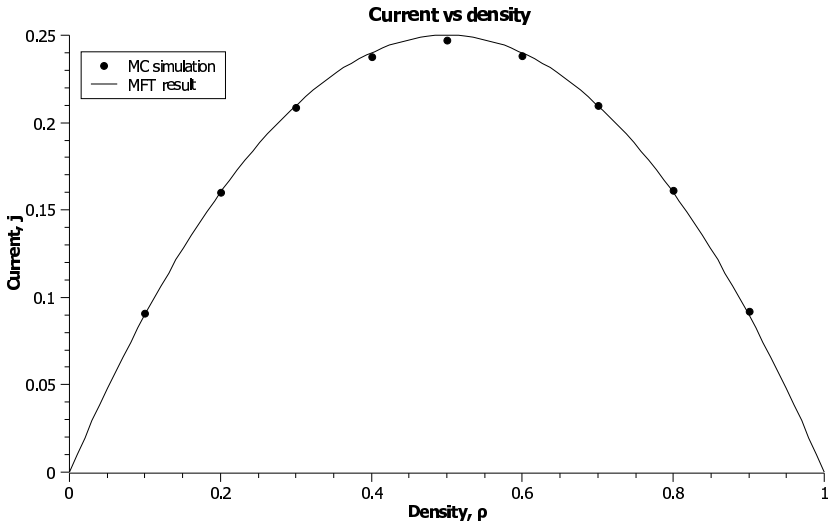

Figure 3.15: Current vs density plot for the 100x100 lattice.

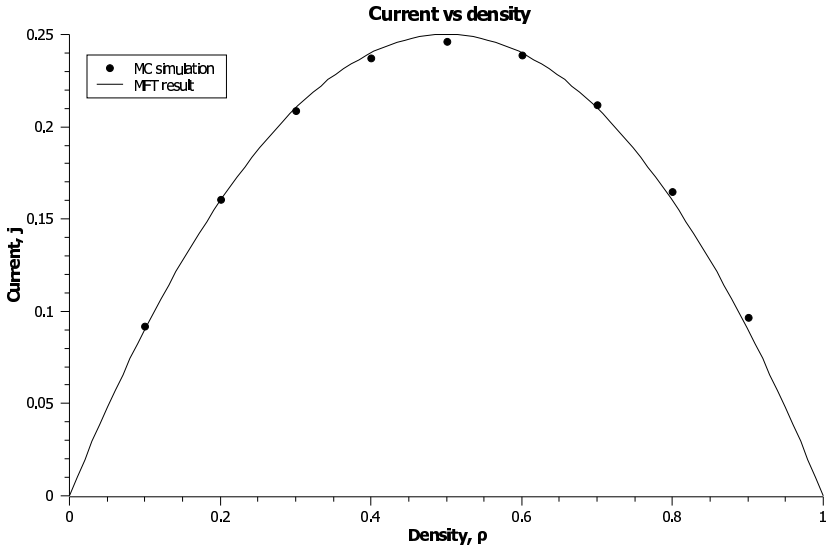

Figure 3.16: Current vs density plot for the 200x200 lattice.

3.4 Coexistence Line.

A system poised at the coexistence line will contain both the low-density phase and the high-density phase, separated by a domain wall, as described by Eq. (3.8). Figures 3.17 and 3.18 show the simulation results for the density profile in the open system where $\alpha = \beta = 0.3$. As we can see, for each run domain wall is located at the different positions. This can be explained by the statistical fluctuations in the rate of entrance and exit of the particles from the system. Those rates are controlled by the random number generator, described in the Appendix A. These two independent events will cause the number of particles in the system to vary, which can be accommodated easily by having the domain wall move back and forth. The number of particles in the system affects where the domain wall is. This effect could be suppressed by changing the boundary conditions, so that the entry and departure of particles from the system were correlated – for example, by using periodic boundary conditions connecting the front and back edges, but with a low probability of crossing this boundary. Results of this simulation are presented below. This would keep the number of particles in the system constant, eliminating the wall motion.

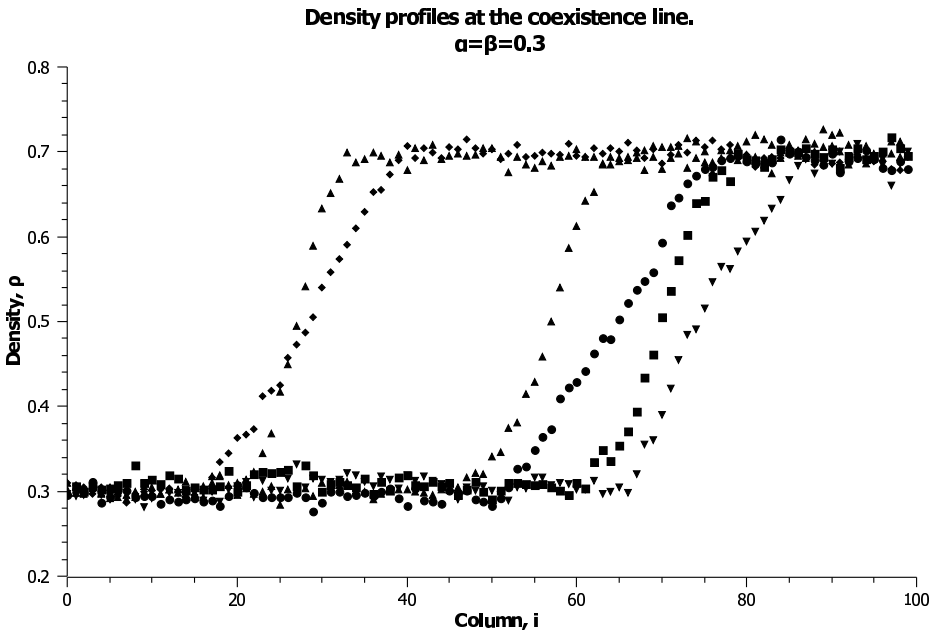

Figure 3.17: Open 100x100 system at the coexistence line. Data from 6 independent runs.

Next we will consider completely periodic lattice with fixed number of particles.

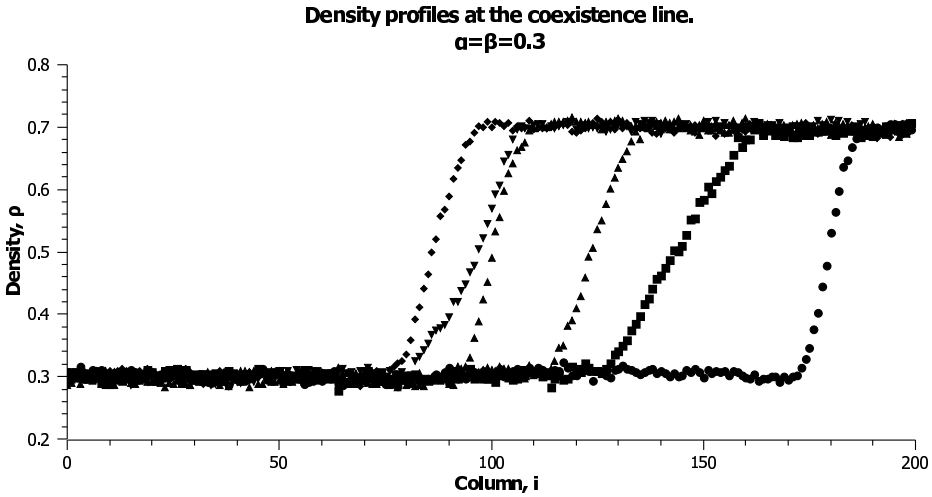

Figure 3.18: Open 200x200 system at the coexistence line. Data from 6 independent runs.

To observe the domain wall we need to create a barrier for the particles to jump from the right edge to the left edge. Following data was generated for three lattices (50x50, 100x100 and 200x200) with the barrier $\gamma = 0.3$.

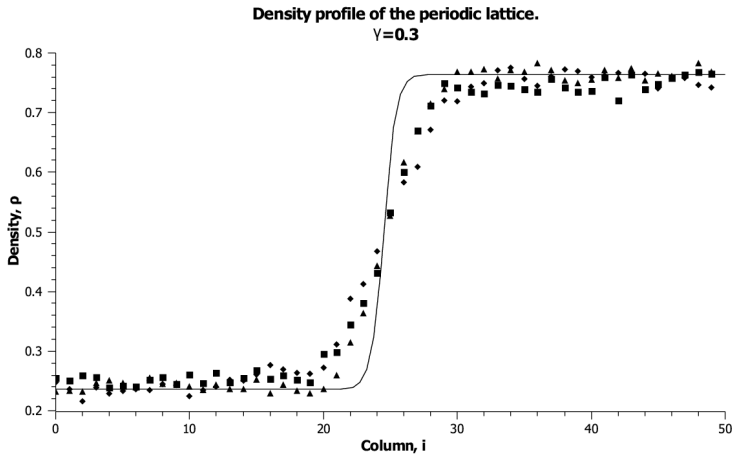

Figure 3.19: Density profile of the periodic 50x50 lattice with the barrier.

On the presented graphs (Figures 3.19, 3.20, 3.21) we showed data of three independent runs for each lattice and compare the MFT result with simulation. As we can see theory and simulation are in good agreement away from the domain

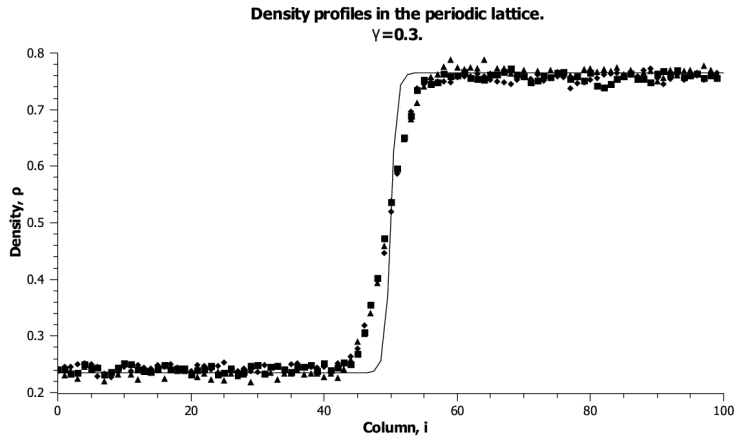

Figure 3.20: Density profile of the periodic 100x100 lattice with the barrier.

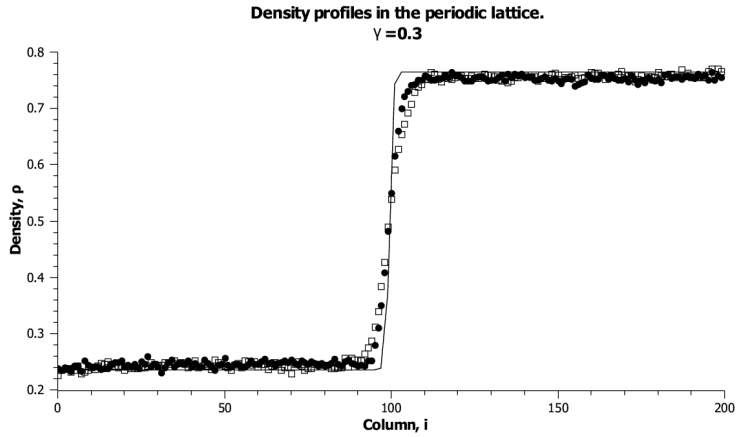

Figure 3.21: Density profile of the periodic 200x200 lattice with the barrier.

wall. However, in the center the theoretical curve is sharper then the curve from the simulation. This is due to some combination of the effects:

1. The domain wall may not be straight. This has origin similar to the previous effect, but can't be controlled by fixing the boundary conditions. Unlike domain walls in thermodynamic systems, there is no way to define an interfacial tension; to the extent that the wall is straight it arises from the particle statistics. From this point of view, it is interesting that the density profile is as abrupt as it is, since the mechanism that straightens the wall will be lateral correlations between particles that the mean field theory doesn't even consider!

We tried looking at snapshots of particle positions and short-run time averages to see what the domain wall looks like, but it is surprisingly hard to see at the particle level (where the "density" at a site is either zero or unity).

2. The correlation length might be larger than the mean-field result. This could be tested separately, in a simpler context.

On the next graphs we show the sensitivity in the the position of the domain wall to imbalances in the rate at which particles enter and leave the system.

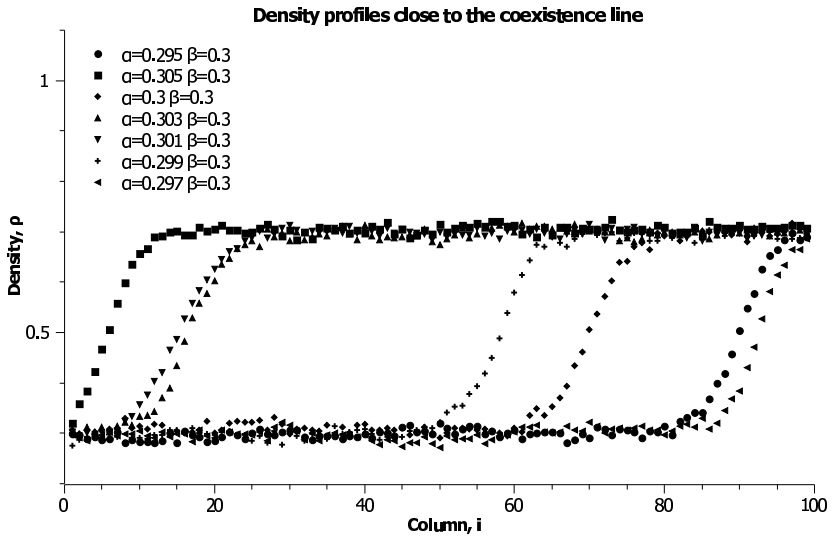

Figure 3.22: Density profiles of the open 100x100 lattice close to the coexistence line.

When $\alpha < \beta$ the low-density phase dominates; the density in most of the system is given by $\rho = \alpha$, and the domain wall is closer to the right edge. For $\alpha > \beta$ the high-density phase dominates; the density in most of the system is given by $\rho = 1-\beta$, and the domain wall is closer to the left edge.

The lack of symmetry between these graphs (for example, density profiles for $\alpha = 0.299, \beta = 0.3$ and $\alpha = 0.301, \beta = 0.3$ should be symmetric) is explained by the same reasons as the not fixed position of the domain wall in the coexistence line.

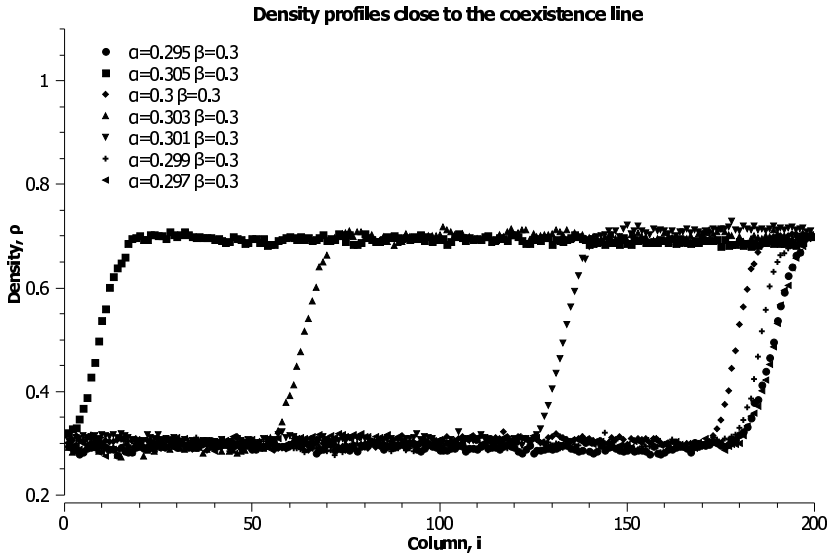

Figure 3.23: Density profiles of the open 200x200 lattice close to the coexistence line.

The symmetry is missing because of the motion of the domain wall.

Chapter 4

Extended Particles (Breaking the Particle-Hole Symmetry)

4.1 Mean-Field Theory

The ASEP models that have been studied previously in this work assume that a particle occupies just one site. In this case the process of moving a particle to the right can be equally well described as a vacancy moving to the left. This leads to a symmetry of the problem, in which $x \to L-x$, $\rho \to (1-\rho)$, $j \to -j$, and $\alpha \to \beta$. This underlies the symmetry of the dependence of j on ρ (Figure 2.3) and the symmetry (in α and β) of the phase diagram (Figure 2.2).

Symmetry is interesting and useful, because it simplifies a problem, but it can also hide the general behavior. So we want to look at models that lack this symmetry, to see if any new features arise. This can be done in one dimension by having particles that occupy M sites instead of just one, but it is a bit artificial, since in many respects it is just the one-site model with a redefinition of the coordinate system, so that the N^{th} particle at x acquires the new coordinate $x + (N-1)(M-1)$; a particle moving forward is still equivalent to a vacancy jumping over the particle. In two dimensions, the introduction of extended particles that exclude other particles from several contiguous sites destroys the symmetry completely, because the motion of one particle is equivalent to the correlated motion of several vacancies.

To break this symmetry any shape of particles larger then one site can be taken. We will concider two models with two different shapes of particles.

4.1.1 Horizontally Extended Particles.

First we considered model where particles occupy two horizontally adjacent cells with coordinates (x, y) and $(x+1, y)$ (referred to as "the particle at (x, y)"). A fragment of a lattice with this kind of particles is shown in Figure 4.1. One of the applications of this kind of model is to construct a model of traffic flow which involves large vehicles (that occupy more space than regular cars). Also it is clearly relevant to

understanding how proteins migrate through a gel during electrophoresis.

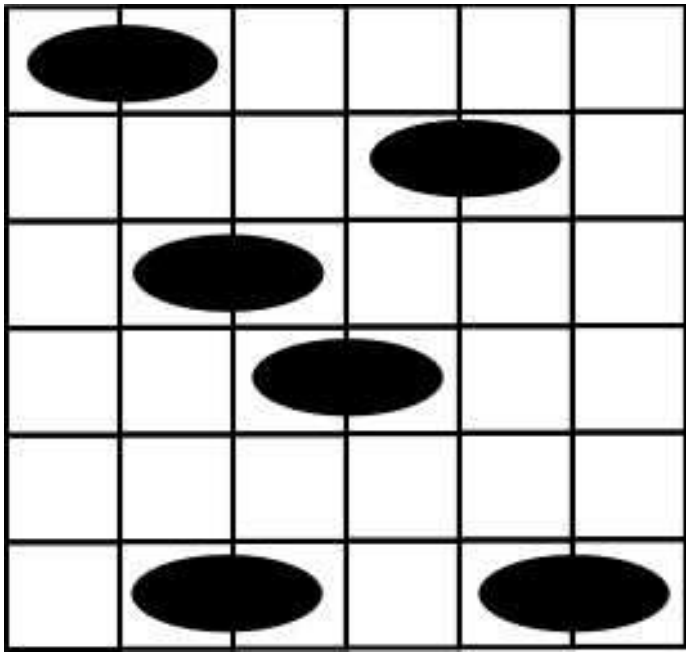

Figure 4.1: Fragment of the lattice with horizontally extended particles.

With this kind of particles we will allow all sites (and not just one sublattice) to be occupied, and allow particles to move from one sublattice to the other, so that the particle at (x, y) can move to $(x+1, y)$ as well as to $(x+1, y+1)$ and $(x+1, y-1)$. The system will be connected periodically in both horizontal and vertical directions (i.e. the case $\gamma = 1$ of the "closed" system).

We will construct a mean-field theory as previously. We will define $\rho(x, y)$ to be the probability that there is a particle that occupies the two sites (x, y) and $(x+1, y)$. Note that the density defined this way cannot exceed $\frac{1}{2}$: this density is distinct from the "coverage density" which is the fraction of sites that are not accessible (it is twice as large as the density for this kind of particle).

The mean-field assumption is that knowing the location of one particle tells us nothing about the locations of the remainder, except that two particular sites are now inaccessible to them.

According to the mean-field theory assumption, the probability that a particular site is occupied by a particle is ρ. Assume that there is a particle at site (x, y). There are three equal possible directions of the jump: upward-right, right and downward-right. Any of these directions may be chosen with probability $\frac{1}{3}$. In order to jump to the neighboring row there should be one or two adjacent vacancies. Next we will

calculate the probability to have those vacancies so the particle can jump.

The particles along any row will obey a kind of Poisson statistics. Consider any particle. The probability that it will be followed by n or more vacant sites will be called $F(n)$. Evidently, $F(0) = 1$, and we will assume there are no correlations between particle positions, so that $F(n+1) = qF(n)$, where q is a parameter, so that requiring one more vacancy decreases the probability of this occurring by a constant ratio q. Then

$$F(n) = q^n. \tag{4.1}$$

Next we define a function $Q(n)$ to be the probability of having exactly n vacancies in a row. We can see that

$$Q(n) = F(n) - F(n+1) = (1-q)q^n. \tag{4.2}$$

The average spacing between particles is:

$$\begin{aligned} D &= 2 + \sum_{n=0}^{\infty} nQ(n) \\ &= 2 + \sum_{n=0}^{\infty} (1-q)nq^n \\ &= \frac{2-q}{1-q}. \end{aligned} \tag{4.3}$$

By definition this is equal to $\frac{1}{\rho}$, so

$$\rho = \frac{1-q}{2-q}, \tag{4.4}$$

or

$$q = \frac{1-2\rho}{1-\rho}. \tag{4.5}$$

Finally we need to know the probability that two adjacent sites are vacant. The situation is illustrated in Fig. 4.2, where the box indicates the pair of sites being considered. There is a particle somewhere in front of the pair of sites, and a string of vacancies that extends past the sites.

The precursor particle can be any distance m away from the target pair of sites,

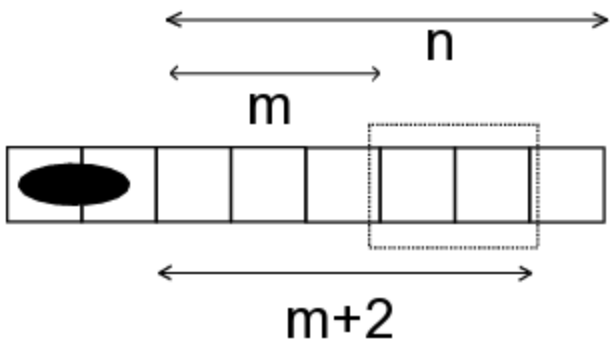

Figure 4.2: Row of the vacancies that cover the sites in question.

and so the probability of this occurrence is

$$\begin{aligned} P &= \rho \sum_{m=0}^{\infty} F(2+m) \\ &= \rho \sum_{m=0}^{\infty} q^{2+m} \\ &= \frac{(1-2\rho)^2}{1-\rho}. \end{aligned} \tag{4.6}$$

where Eq. (4.5) has been used to eliminate the parameter q.

Now we are ready to calculate the probability that particle jumps in various directions can occur. The possible jumps for one particle are shown in Fig. 4.3.

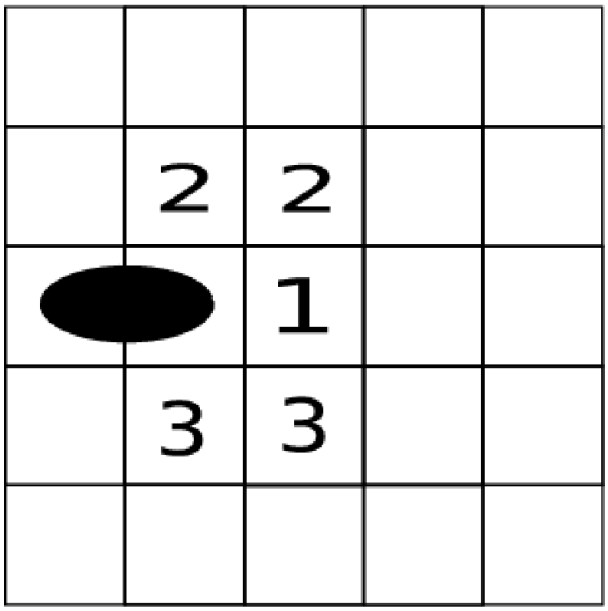

Figure 4.3: Possible jumps of the horizontally extended particle.

Jumps along a row (case 1) require the presence of a particle and one (or more) vacancies following it, which has probability $\rho F(1)$; jumps to another row (cases 2 and 3) require having a particle and a pair of vacancies on the target row, which has probability ρP. The number current density is the average jump rate, which is given by

$$\begin{aligned} j_n &= \frac{1}{3}\rho\frac{1-2\rho}{1-\rho} + \frac{2}{3}\rho\frac{(1-2\rho)^2}{1-\rho} \\ &= \frac{\rho(1-2\rho)(3-4\rho)}{3(1-\rho)}. \end{aligned} \tag{4.7}$$

Since the extended particles are twice as massive as the previous particles (having two parts instead of one), and the motion of one particle involves the displacement of two vacancies, we prefer to define the mass current density, which is twice as large as the number current density:

$$j = \frac{2\rho(1-2\rho)(3-4\rho)}{3(1-\rho)}. \tag{4.8}$$

4.1.2 Vertically Extended Particles.

As a second model we will consider particles that occupy two vertically adjacent sites. with coordinates (x, y) and $(x, y+1)$, and refer to this as the "particle at (x, y)" (a fragment of the lattice with this kind of particles can be seen on Fig. 4.4).

In this model particles are again allowed to move in three directions (upward-right, right and downward-right). Therefore there is no division into two sublattices. We will derive the current in the system under the same assumptions that were used in previous model of extended particles. The definitions of the functions $F(n)$ and $Q(n)$ (Eq. (4.1) and Eq. (4.2)), but now these functions describe the statistics of the vacancies in a column.

In order for the particle to jump to the next row there should be two adjacent vacancies at that row (which allows particle to jump up-right, right or down-right). In the previous section we already calculated the probability to have two adjacent vacancies (Eq. (4.6)). This configuration of vacancies is needed for the particle to jump in any allowed direction. Now we can write down the expression for the particle

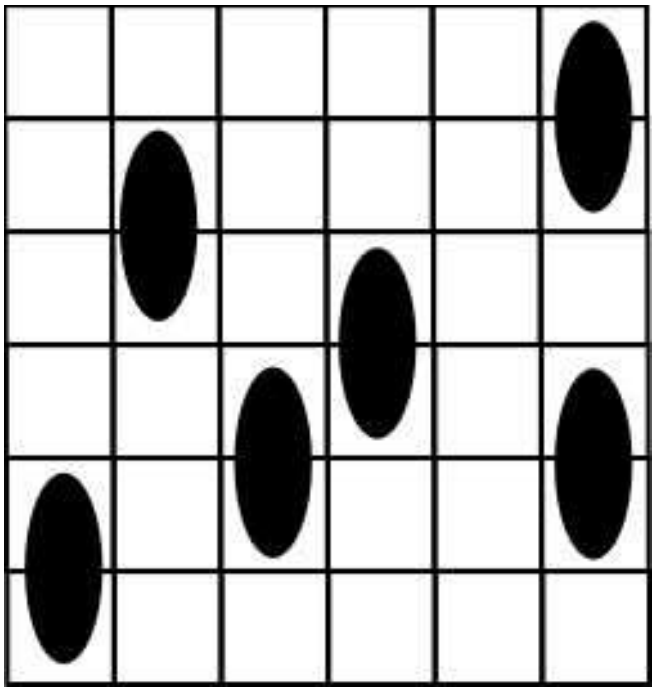

Figure 4.4: Fragment of the lattice with vertically extended particles.

current density:

$$j_n = \rho \frac{(1-2\rho)^2}{1-\rho}. \tag{4.9}$$

In order to get mass current density we multiply right-hand side of this expression by 2, because a jump of one particle is equivalent to the change of the position of two occupied sites:

$$j = 2\rho \frac{(1-2\rho)^2}{1-\rho}. \tag{4.10}$$

4.2 Simulation Results.

To simulate this model we studied 50x50, 100 x 100 and 200x200 square lattice with periodic boundary conditions in all directions. The simulation was run for 10^5 MC steps for 50x50 and 100x100 lattices and 5×10^4 for 200x200 lattice.

4.2.1 Horizontally Extended Particles.

The first three graphs show the relationship of the current to the density of the particles. We observe that the maximum current density (which will still be the critical current density that distinguishes the maximum current phase from the high and low density phases) is no longer $j = \frac{1}{4}$, nor is the corresponding critical density

at $\rho = \frac{1}{2}$.

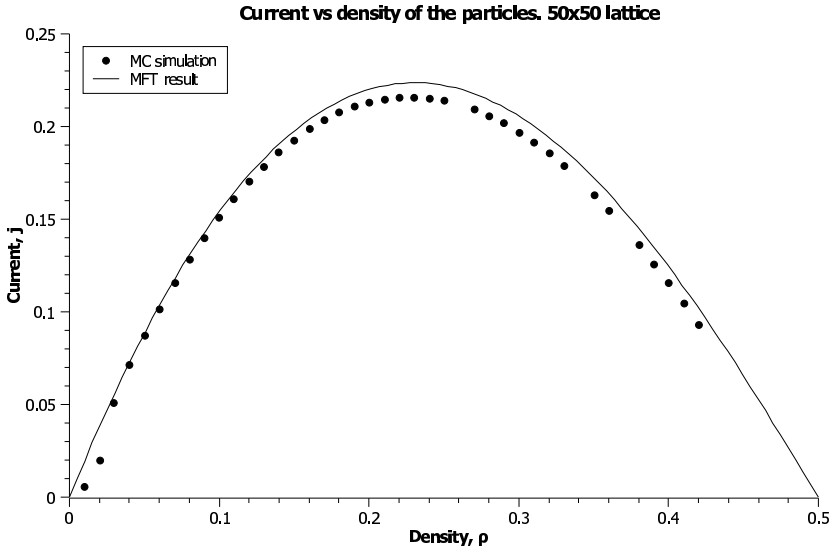

Figure 4.5: Dependency of the current on the density in the 50x50 system with horizontally extended particles.

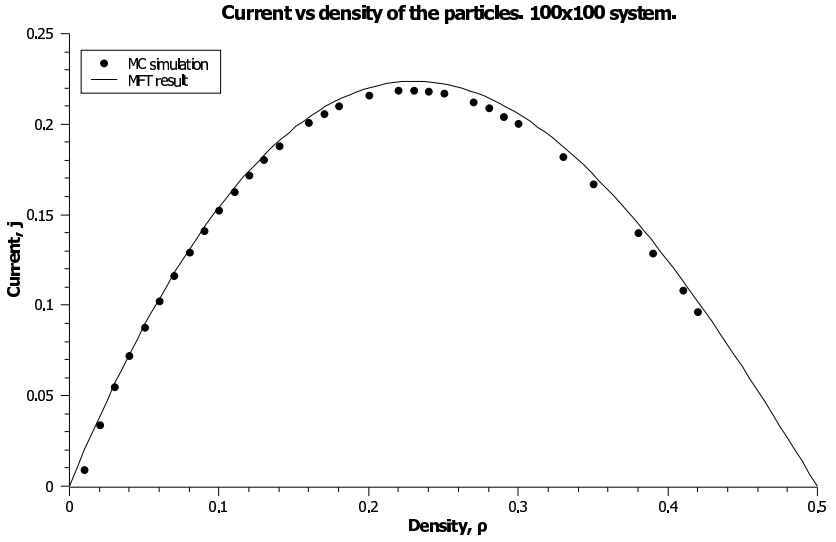

Figure 4.6: Dependency of the current on the density in the 100x100 system with horizontally extended particles.

The MFT predictions and the simulation results are in good agreement in all cases. Below we compare some numerical values of the MFT and simulations (critical values of density and current and values of j for one particular value of the density). Of course, the MFT values do not depend on the size of the system. The MFT values

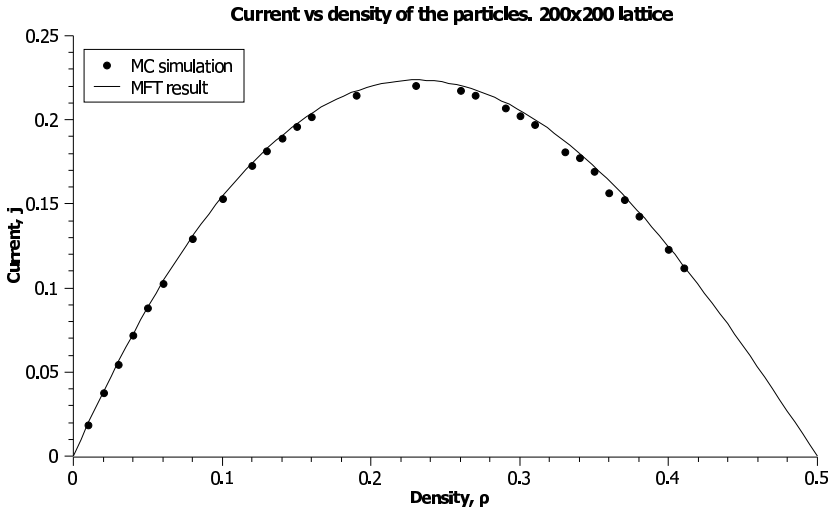

Figure 4.7: Dependency of the current on the density in the 200x200 system with horizontally extended particles.

for the critical density and current can be found by maximizing Eq. (4.7), which gives $\rho_c = 0.2306$ and $j_c = 0.2236$. Also from Eq. (4.7) we get that for $\rho = 0.1$ $j = 0.1541$. Now we compare these values with the values obtained from the simulations:

- For 50x50 lattice we have $\rho_c = 0.2353$ (per cent difference with the MFT value is equal to 2.02%. Critical value of the current is $j_c = 0.2182$ (2.44% difference from the MFT). If $\rho = 0.1$, $j = 0.1509 \pm 7 \times 10^{-5}$ (2.1% different from the MFT).

- For 100x100 lattice $\rho_c = 0.2361$ (per cent difference is 2.37%) and $j_c = 0.2206$ (1.35% difference). If the density of particles is $\rho = 0.1$, $j = 0.1524 \pm 4.5 \times 10^{-5}$ (1.11% difference).

- For 200x200 lattice $\rho_c = 0.2359$ (2.27% difference) and $j_c = 0.2214$ (1.46% difference). For $\rho = 0.1$ $j = 0.1531 \pm 1.5 \times 10^{-5}$, which gives 0.45% difference with the MFT value for this density.

The phase diagrams for the ASEP model with horizontally extended particles are shown on Fig. 4.8, 4.9, 4.10.

The phase diagrams are qualitatively similar to the ASEP system with particles that occupy one lattice site, in that the system can be in the same three states: low

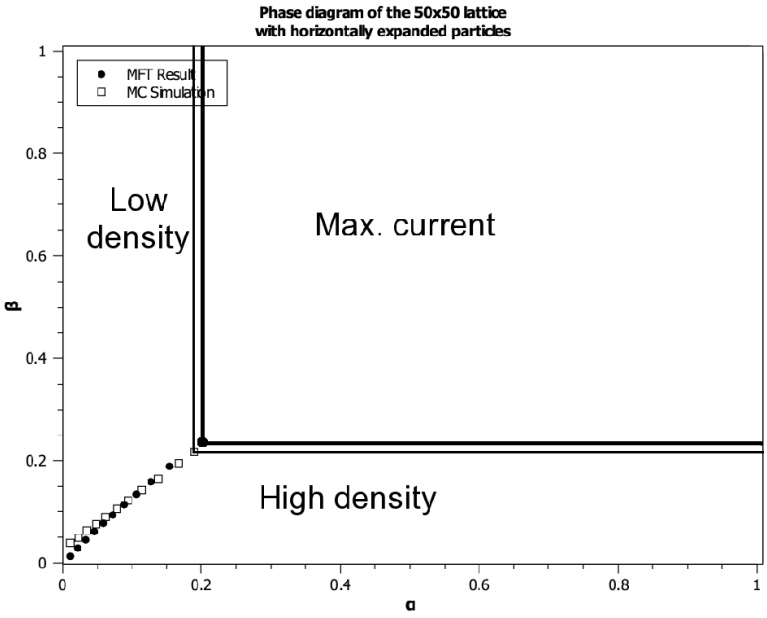

Figure 4.8: Phase diagram for the 50x50 system with horizontally extended particles.

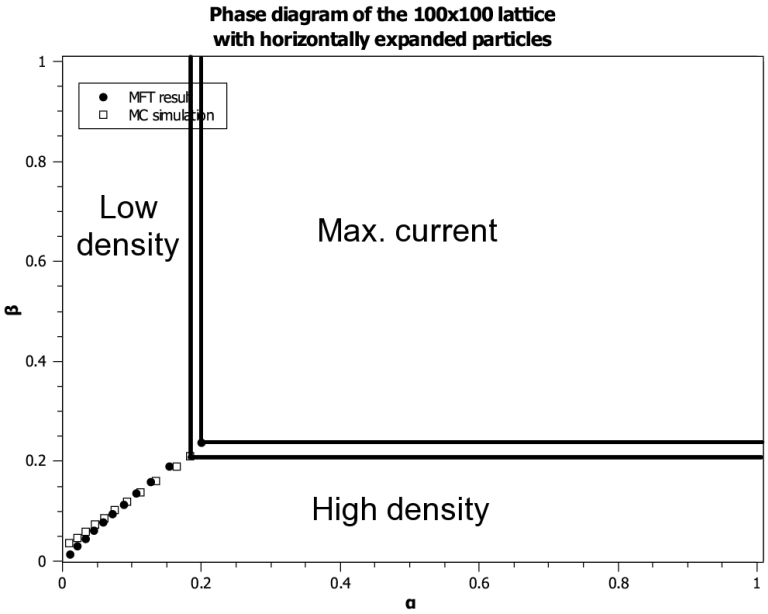

Figure 4.9: Phase diagram for the 100x100 system with horizontally extended particles.

density, high density and maximal current phases. They differ significantly in that the coexistence line between high and low density phases is no longer a line with the slope equal to 1. Of course, the critical density of the system is also different. For single-site particles the critical density and the shape of the coexistence line were determined by the hole-vacancy symmetry, which is no longer present.

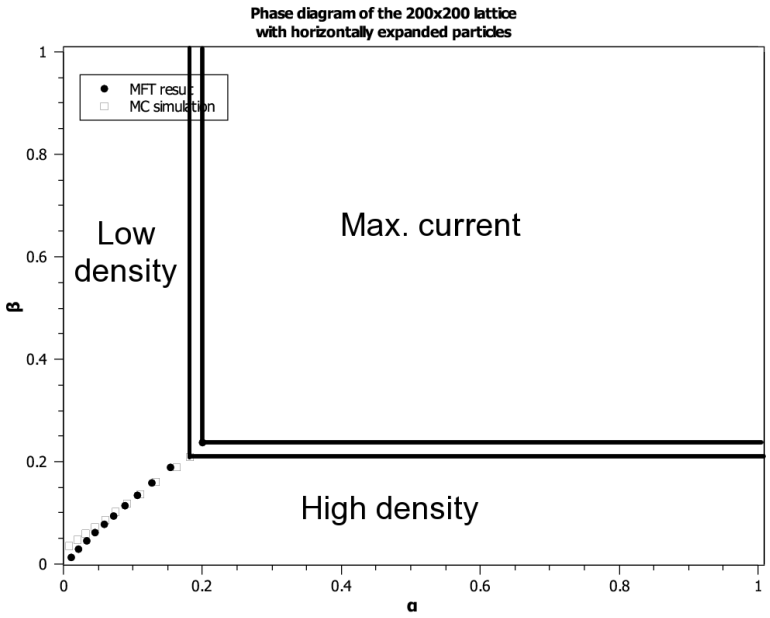

Figure 4.10: Phase diagram for the 200x200 system with horizontally extended particles.

The phase diagrams predicted by MFT also differ from the regular 2D model phase diagrams in that the coexistence line no longer has constant slope. The MFT phase diagrams are in a good agreement with the diagrams obtained from MC simulations.

4.2.2 Vertically Extended Particles.

First we compare dependency of the current on the density of particles. Below are the graphs that demonstrate MFT result (Eq. (4.10)).

Next we present and compare numerical results for critical values of current, density and the value of current for one particular value of the density. From MFT one can calculate that $\rho_c = 0.19$ and $j_c = 0.09$. If $\rho = 0.1$, current is equal to $j = 0.071$. Now consider these values given by MC simulation for each lattice separately.

- For 50x50 lattice $\rho_c = 0.18$ (5.4% per cent difference with MFT) and $j_c = 0.091$ (which is 1.1% per cent difference with MFT). When $\rho = 0.1$, $j = 0.073$ (2.8% per cent difference).

- For 100x100 lattice $\rho_c = 0.18$ (5.4% per cent difference with MFT) and $j_c =$

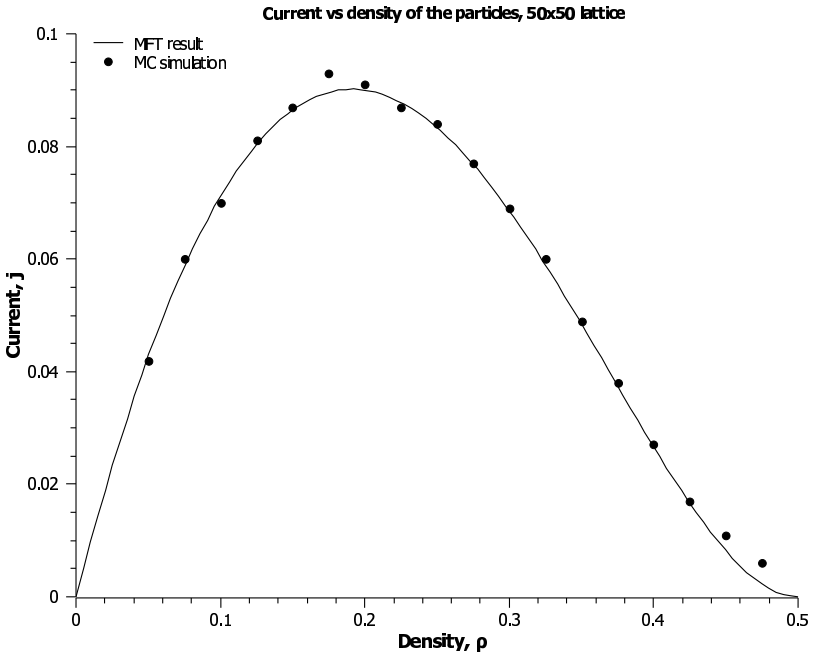

Figure 4.11: Dependency of the current on the density in the 50x50 system with vertically extended particles.

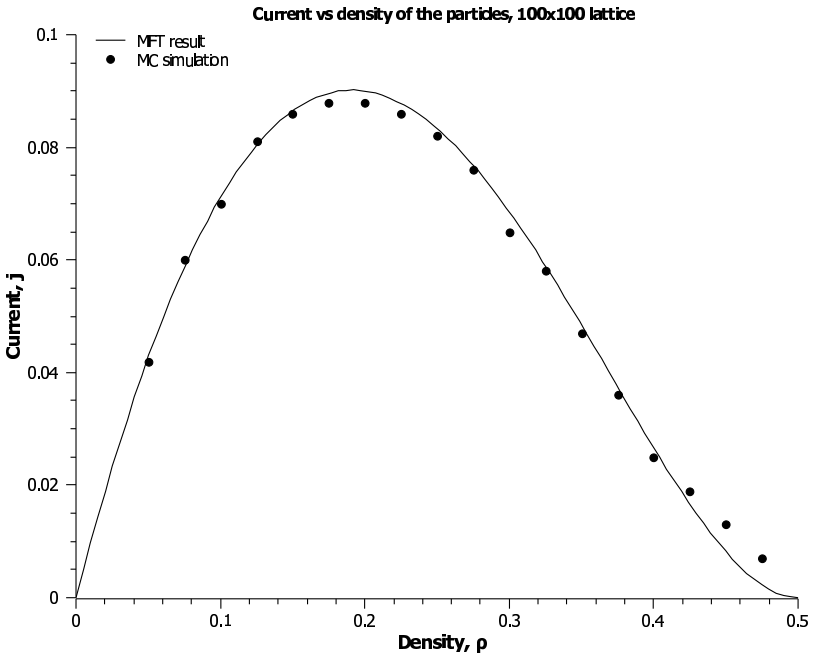

Figure 4.12: Dependency of the current on the density in the 100x100 system with vertically extended particles.

0.089 (1.1% per cent difference with MFT). For $\rho = 0.1$ $j = 0.072$ (which gives 1.4% per cent difference with MFT result).

- For 200x200 lattice we have $\rho_c = 0.18$ (5.4% per cent difference with MFT),

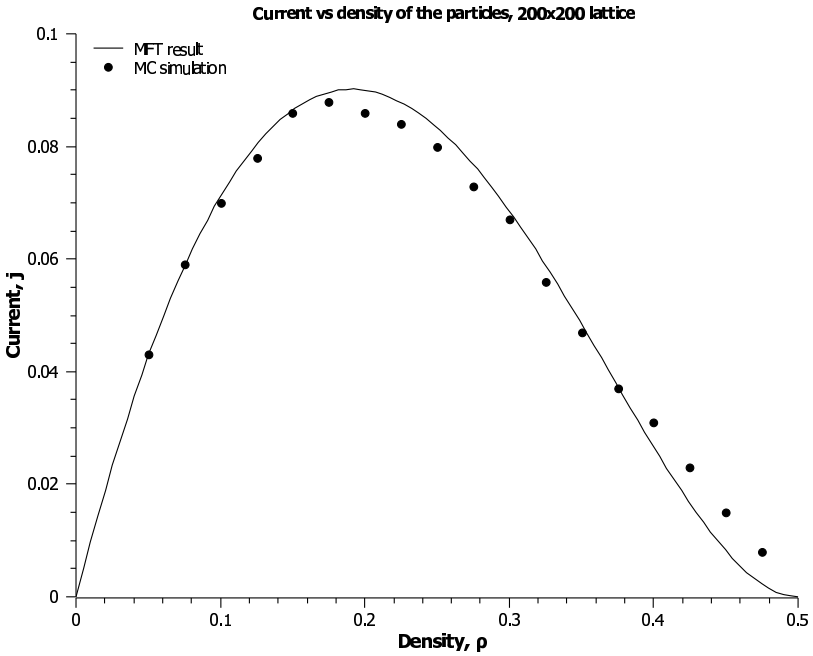

Figure 4.13: Dependency of the current on the density in the 200x200 system with vertically extended particles.

$j_c = 0.087$ (3.4% per cent difference with MFT). If $\rho = 0.1$, $j = 0.071$, which exactly the same result with MFT.

Next we present phase diagrams of the system with vertically extended particles (Figures 4.14, 4.15 and 4.16).

According to MFT, the current density approaches zero quadratically in $(1 - 2\rho)$ (simply because this requires having two vacancies for anything to happen). The simulation doesn't quite support this, suggesting that the vacancies are correlated. A possible explanation is that when a particle moves, it leaves behind a pair of adjacent vacancies. This feature affects the shape of the transition line between the low- and high-density phases; the quadratic feature in $j(\rho)$ would cause a parabolic shape for the transition line near small α and β.

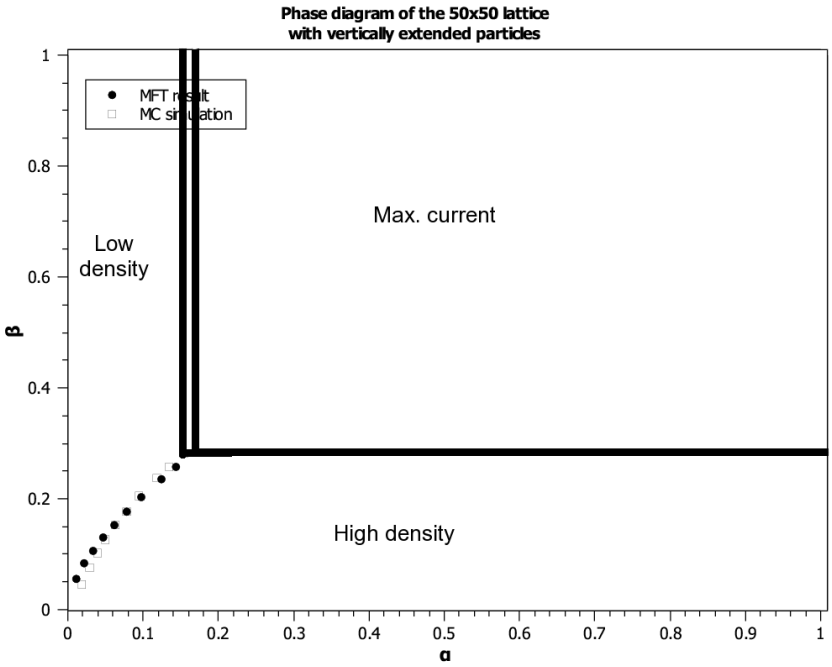

Figure 4.14: Phase diagram for the 50x50 system with vertically extended particles.

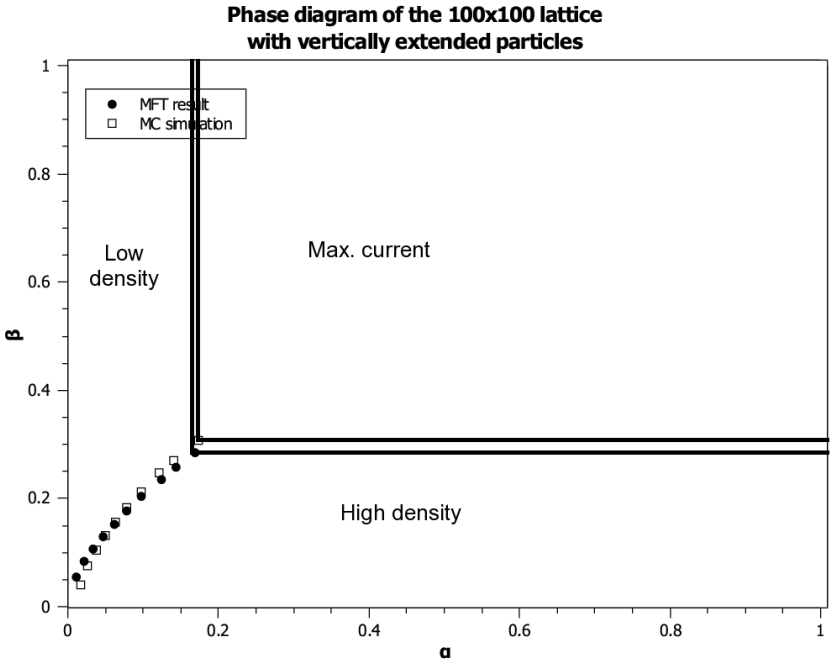

Figure 4.15: Phase diagram for the 100x100 system with vertically extended particles.

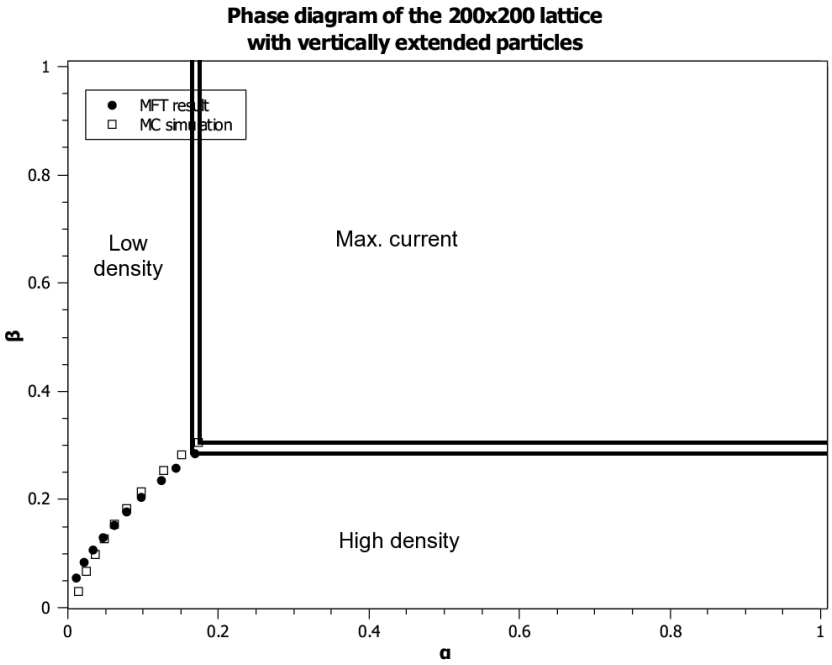

Figure 4.16: Phase diagram for the 200x200 system with vertically extended particles.

Chapter 5

2D ASEP Model with Vertical Particle Drift

Now we modify the 2D ASEP model defined above so that we break the symmetry $y \to -y$, by making the probability p to jump upward-right different from the probability $1-p$ to jump downward-right. This will introduce a vertical bias for the motion of the particles, resulting in a net current in the vertical direction.

This appears to be the first example of a model where two-dimensional particle interaction must be taken into account, in contrast with all previous models where MFT was reduced to one dimension.

5.1 Mean-Field Theory.

To calculate the current at the site (x, y) we can calculate currents through the vertical planes located at the distance of half a lattice spacing to the both sides from the site and then average them. Here we are applying the same mean-field approximations made above for the regular 2D model and substitute probability of the site to be occupied by its average value, i.e. average density. Starting from the right plane we can write:

$$j_x(x+\frac{1}{2}) = (1-p)\rho(x,y)(1-\rho(x+1,y+1)) + p\rho(x,y)(1-\rho(x+1,y-1)), \quad (5.1)$$

and

$$j_y(x+\frac{1}{2}) = (1-p)\rho(x,y)(1-\rho(x+1,y+1)) - p\rho(x,y)(1-\rho(x+1,y-1)), \quad (5.2)$$

where subscript of j indicates the correspondent component of the current.

Using the Taylor series expansion for the function of two variables and keeping the terms up to the first order we get:

$$j_x(x+\frac{1}{2}) = \rho(1-\rho) - \rho(\frac{\partial\rho}{\partial x} + (1-2p)\frac{\partial\rho}{\partial y}), \quad (5.3)$$

and

$$j_y(x+\frac{1}{2}) = (1-2p)\rho(1-\rho) - \rho((1-2p)\frac{\partial\rho}{\partial x} + \frac{\partial\rho}{\partial y}). \tag{5.4}$$

Similarly we can get the currents through the second plane located to the left from the site.

$$j_x(x-\frac{1}{2}) = (1-p)\rho(x-1,y-1)(1-\rho(x,y)) + p\rho(x-1,y+1)(1-\rho(x,y)), \tag{5.5}$$

and

$$j_y(x-\frac{1}{2}) = (1-p)\rho(x-1,y-1)(1-\rho(x,y)) - p\rho(x-1,y+1)(1-\rho(x,y)). \tag{5.6}$$

Using expansion and ignoring high order terms we get:

$$j_x(x-\frac{1}{2}) = \rho(1-\rho) - (1-\rho)(\frac{\partial\rho}{\partial x} + (1-2p)\frac{\partial\rho}{\partial y}), \tag{5.7}$$

and

$$j_y(x-\frac{1}{2}) = (1-2p)\rho(1-\rho) - (1-\rho)((1-2p)\frac{\partial\rho}{\partial x} + \frac{\partial\rho}{\partial y}). \tag{5.8}$$

In order to get the current through the site (x, y) we need to average components of the current calculated above:

$$j_x = \frac{j_x(x - \frac{1}{2}) + j_x(x + \frac{1}{2})}{2}, \tag{5.9}$$

and

$$j_y = \frac{j_y(x - \frac{1}{2}) + j_y(x + \frac{1}{2})}{2}. \tag{5.10}$$

As the result for j_x we get:

$$j_x = \rho(1 - \rho) - \frac{1}{2}\frac{\partial \rho}{\partial x} - \frac{1}{2}(1 - 2p)\frac{\partial \rho}{\partial y}, \tag{5.11}$$

and for j_y:

$$j_y = (1 - 2p)\rho(1 - \rho) - \frac{1}{2}\frac{\partial \rho}{\partial y} - \frac{1}{2}(1 - 2p)\frac{\partial \rho}{\partial x}. \tag{5.12}$$

Far from critical regions (domain walls) we can ignore gradient terms in the current expressions. In this case we can rewrite current components as following:

$$j_x = \rho(1 - \rho), \tag{5.13}$$

$$j_y = (1 - 2p)\rho(1 - \rho). \tag{5.14}$$

Since we didn't change anything regarding motion of the particles in horizontal direction, the relationship between current in that direction and density didn't change and it is the same as it was for the regular system without vertical bias. But as we can see, current in vertical direction depends not only on the density of the particles but also on the probability to jump upward-right.

To get the critical values of density and current one can start from the expressions for the current. Starting with the Eq.(5.13) we can write:

$$\frac{\partial J_x}{\partial \rho} = 0, \tag{5.15}$$

$$\frac{\partial J_x}{\partial \rho} = 1 - 2\rho. \tag{5.16}$$

Combining these two conditions we get:

$$\rho_c = \frac{1}{2}. \tag{5.17}$$

Substituting this value to the Eq.(5.13) we get:

$$J_{xMax} = \frac{1}{4}. \tag{5.18}$$

The same procedure can be applied to the Eq.(5.14):

$$\frac{\partial J_y}{\partial \rho} = (1-2p)(1-2\rho) = 0. \tag{5.19}$$

From this equation we again get the same value for the critical density:

$$\rho_c = \frac{1}{2}. \tag{5.20}$$

Returning to the Eq.(5.14) and using this value of density we get:

$$J_{yMax} = \frac{1}{4}(1-2p). \tag{5.21}$$

5.2 Simulation Results

To test the MFT predictions for the model with vertical asymmetry, simulations were performed for 50x50, 100x100 and 200x200 lattices with periodic boundary conditions at all edges. Initial density of the particles varied from 0.1 to 0.9. Probability to jump up-right is $p = 0.3$.

To verify the theory first we present values of current far from critical densities. For this purpose $\rho = 0.3$ was chosen. At this density MFT results for the components of the current are $j_x = 0.21$ and $j_y = 0.084$. Below we present result of the simulation for three different lattice sizes.

5.2.1 50x50 lattice.

First we present simulation results for the 50x50 lattice. For $\rho = 0.3$ we have: $j_x^{sim} = 0.196 \pm 0.0001$. This is 6.9% difference with the MT result. Vertical component of the current in this lattice is $j_y^{sim} = 0.0784 \pm 5.96 \times 10^{-5}$ (6.9% difference with the MFT value).

Below are the graphs (Fig. 5.1 and Fig. 5.2)which are comparing simulation result for the distribution of the current components vs density of the particles with the MFT results.

According to MFT the ratio between current components j_x and j_y should be a constant value:

$$\frac{j_x}{j_y} = \frac{1}{1-2p}. \tag{5.22}$$

In this particular case, when $p = 0.3$ this ratio is equal to 2.5. To verify this we plot the ratio j_x/j_y vs ρ (Fig. 5.3).

Average value of the ratio and its standard deviation is $\frac{j_x}{j_y} = 2.499 \pm 0.002$.

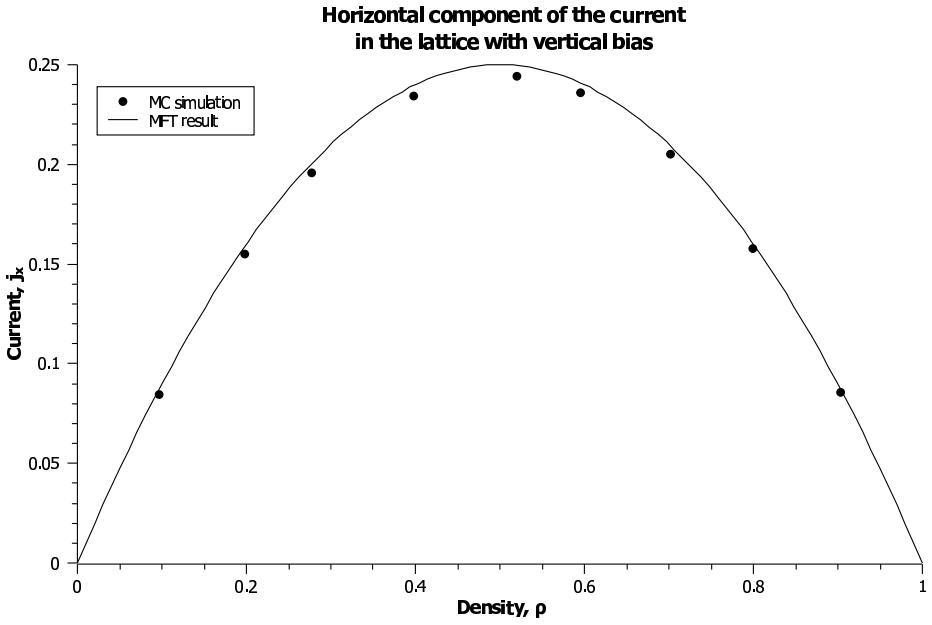

Figure 5.1: Relationship $j_x(\rho)$ for the 50x50 ASEP model with vertical bias of particles. Probability to jump upward-right is $p = 0.3$.

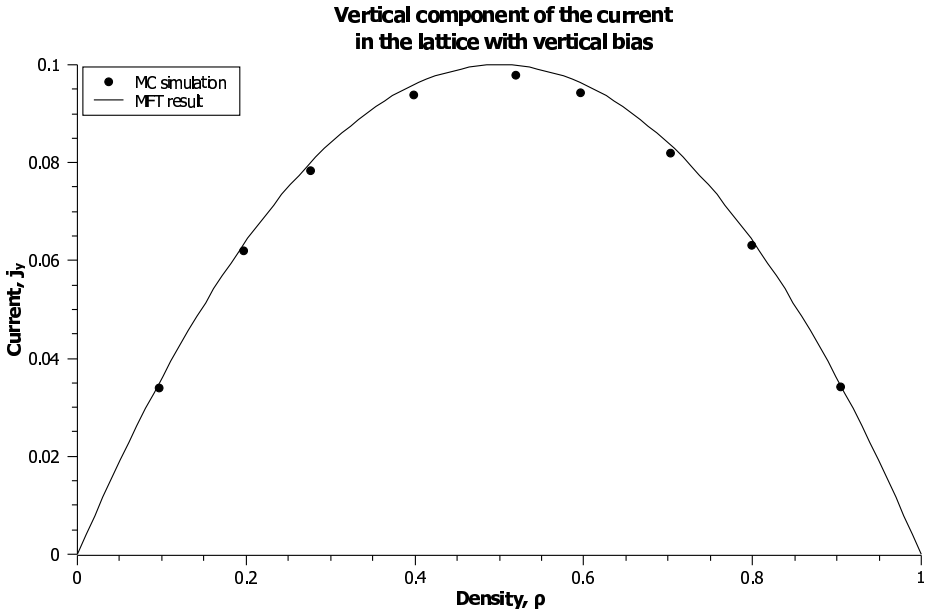

Figure 5.2: Relationship $j_y(\rho)$ for the 50x50 ASEP model with vertical bias of particles. Probability to jump upward-right is $p = 0.3$.

5.2.2 100x100 lattice.

Values for the same density and probability to jump up-right are: $j_x^{sim} = 0.2027 \pm 5.32 \times 10^{-5}$ (that gives 3.54% difference with the result of MFT). For the vertical

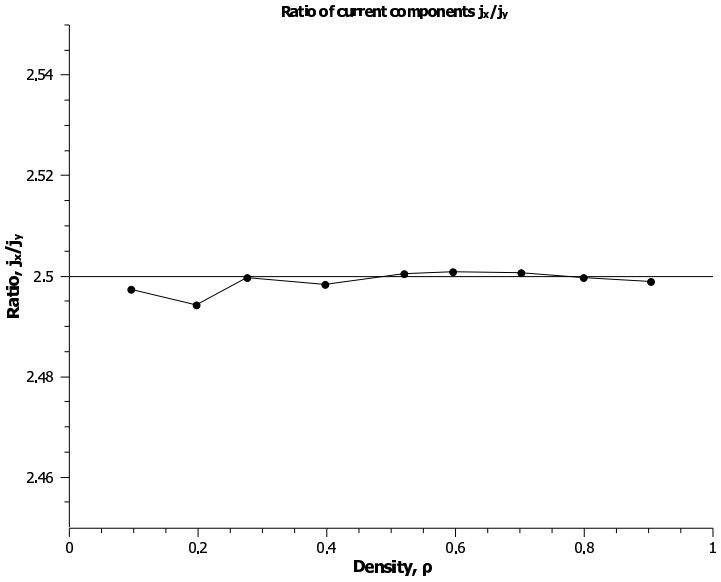

Figure 5.3: Current ratio vs density of the particles in the 50x50 ASEP model with vertical particle drift.

component of the current MFT gives the value $j_y = 0.084$. From the simulation we have $j_y^{sim} = 0.081 \pm 3.75 \times 10^{-5}$ (which is 3.58% difference with MFT result).

Below we present two graphs of the current components where we compare MFT results for the relationship between the current component and the density of the particles in the system and the same result from the MC simulations. As one can see, on both graphs theoretical curves and data sets from simulations are in a good agreement.

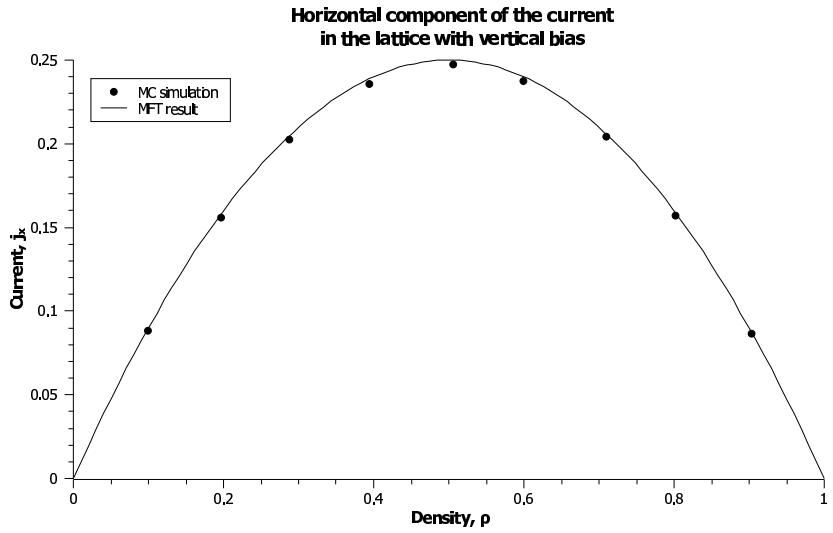

Figure 5.4: Relationship $j_x(\rho)$ for the 100x100 ASEP model with vertical bias of particles. Probability to jump upward-right is $p = 0.3$.

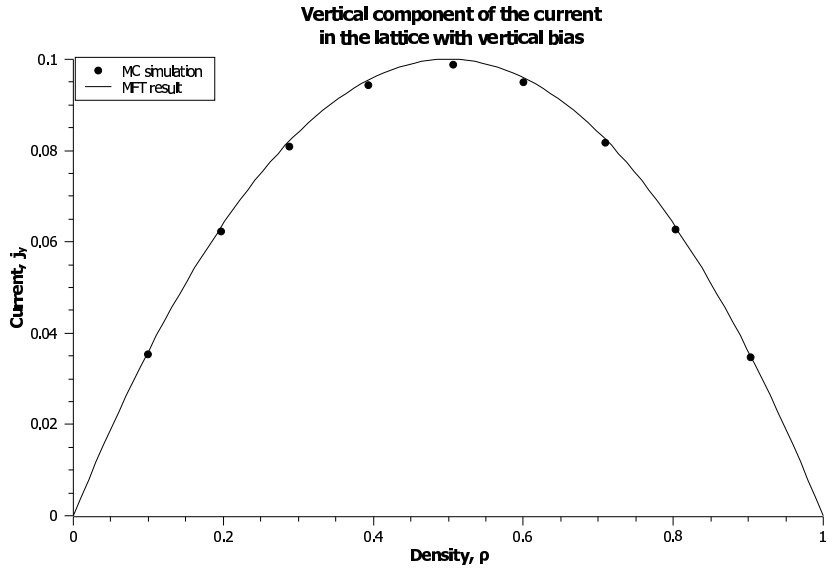

Figure 5.5: Relationship $j_y(\rho)$ for the 100x100 ASEP model with vertical bias of particles. Probability to jump upward-right is $p = 0.3$.

To compare the ratio of the current components to its MFT value we plot them on the Fig. 5.6.

Average value of the data presented on the Fig. 5.6 is $\dfrac{j_x}{j_y} = 2.5 \pm 0.001$.

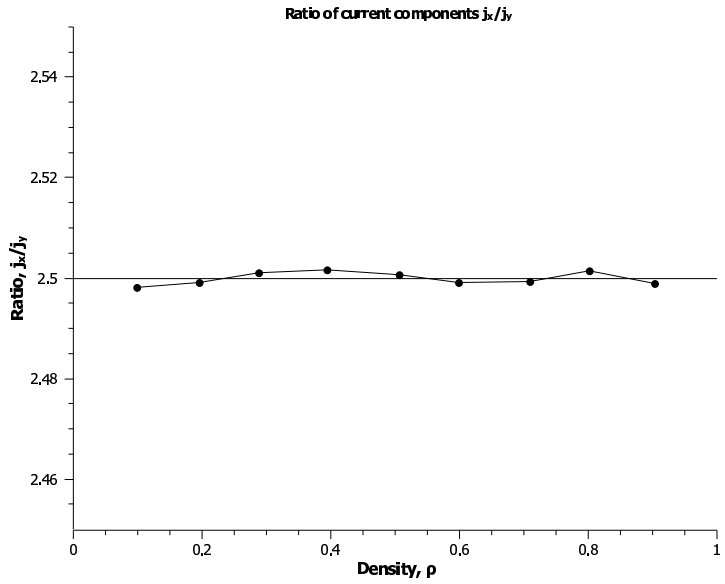

Figure 5.6: Current ratio vs density of the particles in the 100x100 ASEP model with vertical particle drift.

5.2.3 200x200 lattice.

For the 200x200 lattice values current components are as following: $j_x^{sim} = 0.2086 \pm 4.23 \times 10^{-5}$ (that gives 0.68% difference with the result of MFT). For the vertical component of the current we have $j_y^{sim} = 0.0834 \pm 4.57 \times 10^{-5}$ (0.72% difference with MFT result).

Next we present two graphs of the current components calculated in the simulation in comparison with the MFT results for the relationship between the current component and the density of the particles in the system.

The last graph compares the ratio of the current components to its MFT value (Fig. 5.9).

Average value of the data presented on the Fig. 5.9 is $\frac{j_x}{j_y} = 2.5 \pm 0.0007$.

Comparing results of all three simulations and MFT results one can see that as system gets larger, the deviation of the simulation result from the MFT one gets smaller. This can be seen by comparing percent differences between MFT values of current components and currents calculated by the simulation. This can be explained by the fact that while deriving MFT result we made an assumption that the density is homogeneous and there are no density gradients in the lattice. To make density gradients negligibly small we need to have a large system. Hence, the larger the

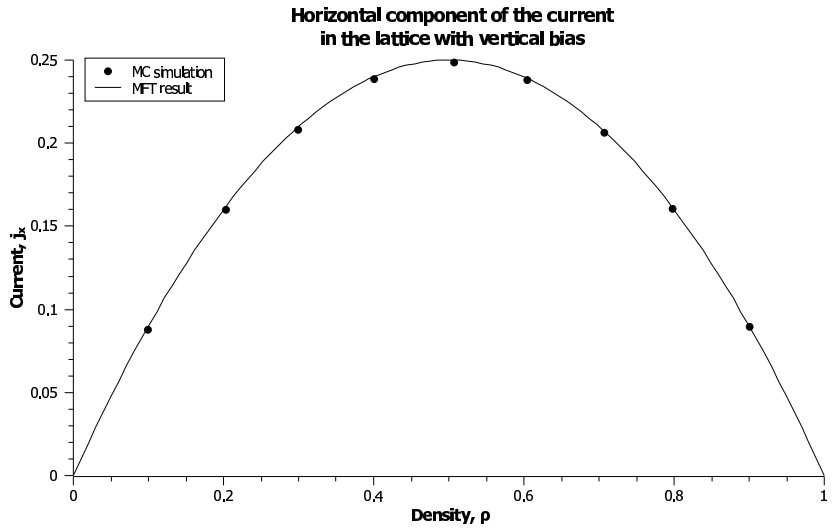

Figure 5.7: Relationship $j_x(\rho)$ for the 200x200 ASEP model with vertical bias of particles. Probability to jump upward-right is $p = 0.3$.

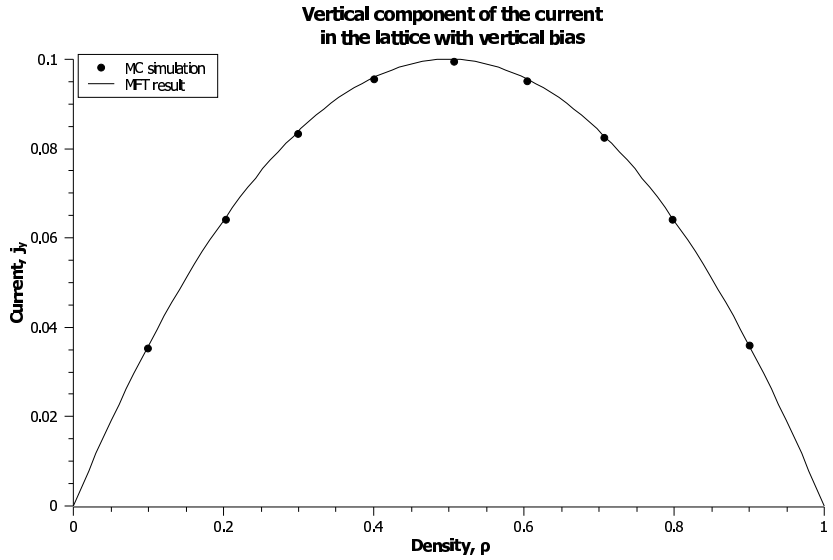

Figure 5.8: Relationship $j_y(\rho)$ for the 200x200 ASEP model with vertical bias of particles. Probability to jump upward-right is $p = 0.3$.

system, the smaller the density gradients and therefore the simulation results are

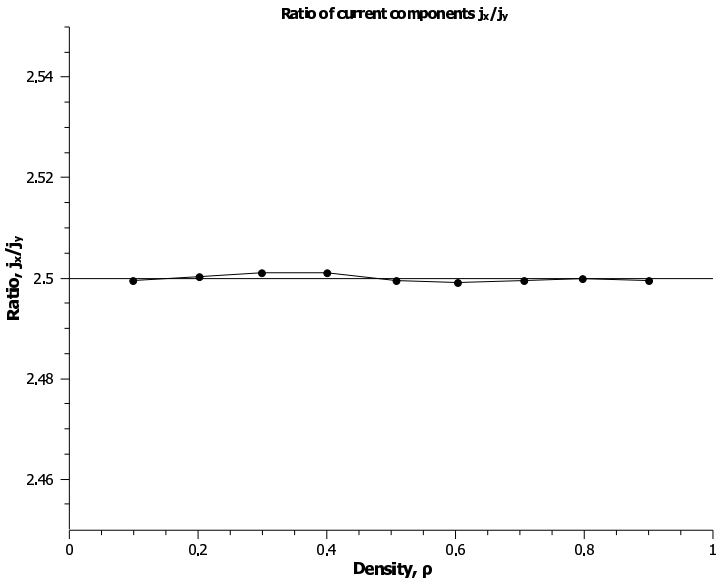

Figure 5.9: Current ratio vs density of the particles in the 200x200 ASEP model with vertical particle drift.

closer to the MFT results.

Chapter 6

Lattice with an Obstacle

In the 2D ASEP model, spatial inhomogeneity can give rise to current inhomogeneity: if we put an obstacle in the system, the current can flow around it. This is quite different from the case of one dimension, where every particle has to pass through every site. At least in principle, the spatial anisotropy of the 2D ASEP model implies that longitudinal and transverse correlations will have different correlation lengths, which might affect the density pattern around an obstacle. Intuitively we would expect that an obstacle will cause a "traffic jam" in front of it, with an excess of the particles, and a "shadow" that is deficient in particles behind it. This problem will be studied by solving the mean-field theory equations and through simulations.

6.1 Mean-field theory

The mean field assumption gives a difference equation for the density

$$\frac{\partial \rho}{\partial t} = [\rho(x-1,y-1)+\rho(x-1,y+1)][1-\rho(x,y)]-\rho(x,y)[2-\rho(x+1,y-1)-\rho(x+1,y+1)]. \tag{6.1}$$

In Chapter 3, this was expanded in gradients to derive a partial differential equation for the density (Eq. (3.7)). For steady state this becomes

$$0 = \frac{\partial^2 \rho}{\partial x^2} + \frac{\partial^2 \rho}{\partial y^2} - 2\frac{\partial \rho(1-\rho)}{\partial x}. \tag{6.2}$$

An obstacle is a region through which the current cannot pass, so that there is some contour where the normal component of the current is zero. This will result in an increase of the density right in front of the obstacle and a "shadow" zone behind it. However, at large distances from the obstacle the density is expected to be only slightly perturbed. We will choose the boundary conditions at large distances so that the density is uniform, and denote it as ρ_∞. At sufficiently large distances ρ is close to ρ_∞, so that we can linearize Eq. (6.2) in the variables $f = \rho - \rho_\infty$, giving

$$-S\frac{\partial\delta(x)\delta(y)}{\partial x} = \frac{\partial^2 f}{\partial x^2} + \frac{\partial^2 f}{\partial y^2} - 2c\frac{\partial f}{\partial x}. \tag{6.3}$$

where $c = 1 - 2\rho_\infty$. The left-hand side is a dipole source of strength S representing the obstacle. This equation can be solved using Fourier transform methods.

Defining

$$f(x,y) = \int f(k_x,k_y)e^{ik_x x + ik_y y}\,\frac{d^2k}{2\pi} \tag{6.4}$$

leads to

$$f(k_x,k_y) = \frac{iSk_x}{k_x^2 + k_y^2 + 2ick_x}. \tag{6.5}$$

Substituting this expression into Eq. (6.4) gives an integral representation of the solution:

$$f(x,y) = S\int \frac{ik_x e^{ik_x x + ik_y y}}{k_x^2 + k_y^2 + 2ick_x}\,\frac{d^2k}{2\pi} = S\frac{\partial}{\partial x}\int \frac{e^{ik_x x + ik_y y}}{k_x^2 + k_y^2 + 2ick_x}\,\frac{d^2k}{2\pi}. \tag{6.6}$$

This integrand is an analytic function of k_x, except for poles at $k + x = -ic \pm i\sqrt{k_y^2 + c^2}$, which are on opposite sides of the real k_x axis. Then according to the Cauchy theorem, we can shift the contour by $k_x \to -ic + k_x$, which gives

$$f(x,y) = S\frac{\partial}{\partial x}e^{cx}\int \frac{e^{ik_x x + ik_y y}}{k_x^2 + k_y^2 + c^2}\,\frac{d^2k}{2\pi}. \tag{6.7}$$

Since the integral is the Fourier integral representation of the solution to the two-dimensional Helmholtz problem with unit source, we can write down the solution:

$$\rho(x,y) = \rho_\infty + S\frac{\partial}{\partial x}(e^{cx}K_0(c\sqrt{x^2+y^2})), \tag{6.8}$$

where K_0 is the modified Bessel function of the second kind.

For large argument, $K_0(r) \approx \dfrac{e^{-r}}{\sqrt{r}}$. Then for $x < 0$, $\rho(x,0) \approx \rho_\infty + Sce^{-2c|x|}$, while for $x > 0$, $\rho(x,0) \approx \rho_\infty - Sc(cx)^{-3/2}$. In the transverse direction we find that $\rho(0,y) \approx \rho_\infty + Sce^{-|cy|}$.

Closer to the origin (where the obstacle is), the linearization will fail. We have been assuming that we can approximate $\dfrac{\partial\rho(1-\rho)}{\partial x} = (1-2\rho)\rho_x$ by $c\rho_x$. However, on the front side of the obstacle we can expect to find a region where $\rho > \dfrac{1}{2}$, and then the replacement of $(1-2\rho)$ by a positive constant is quite questionable. Indeed, the front side of the obstacle is a region where the density is increasing from density less than $\frac{1}{2}$ to greater $\frac{1}{2}$; there could be a domain wall, rather than a smooth transition. We observe that in front of the object, where there is a pile-up, the density will be crossing from $\rho < 1/2$ to $\rho > 1/2$, and the characteristic length scale $\xi \approx \frac{1}{c}$ appears. Behind the obstacle, in the shadow region, the density is everywhere less than critical, and this region is described by a power-law.

The linearization can be avoided, by numerically solving the difference Eq. (6.1), by letting the sites take on continuous values for ρ, and moving a "current" proportional to $\rho(x,y)(1-\rho(x',y'))$ along each bond on each time step. This process rapidly converges to a steady state in which the difference equation is satisfied to high accuracy at every site. Figure 6.1 gives an example.

In this figure the lattice sites are the colored dots; the obstacle is the pair of white dots. The particles are moving from left to right, as usual. The 40 x 40 lattice has periodic boundary conditions, and the average density is 0.30. Sites containing a higher density are shaded red, so that full red means that the density is unity (the site directly in front of the obstacle is full red, because there is no way for particles to leave it); sites with less than average density are shaded blue. We see that there is a dipolar disturbance, as expected.

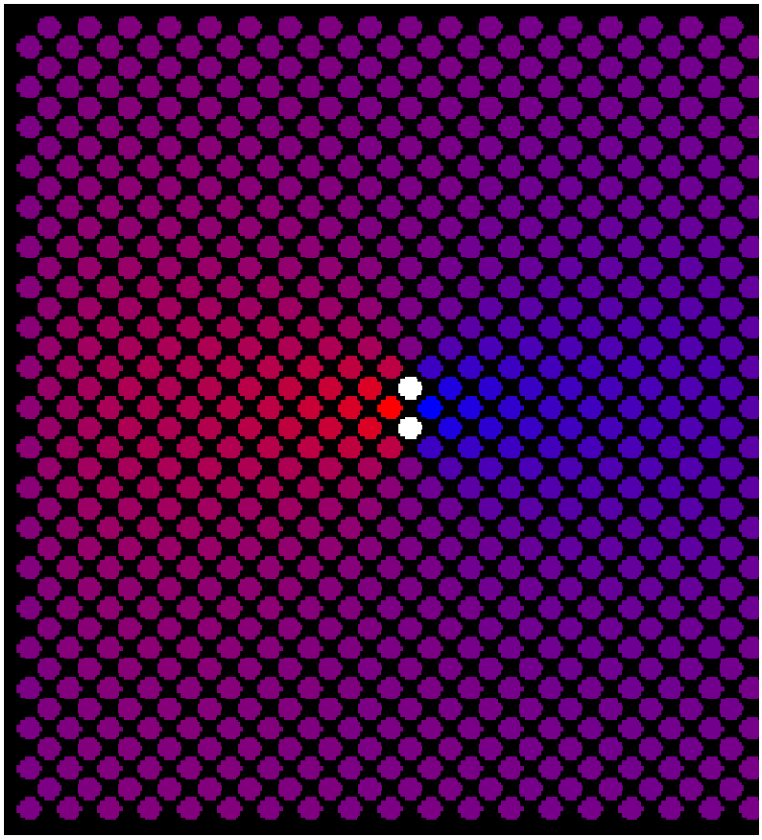

Figure 6.1: Snapshot of the lattice with obstacle.

6.2 Simulation Results

Monte Carlo simulations were also done. It isn't easy to get high accuracy, because a site either contains a particle or it does not; the density is the average of a lot of ones and zeroes. We would need 10,000 independent samples to determine the density to within 1%, and the samples would have to be separated by many thousands of Monte Carlo steps to assure independence (the density shown elsewhere is a column average). Next three figures show the density distributions along the x axis as predicted by the MFT solution, and the density averaged for each column as determined by a Monte Carlo simulation. The obstacle was again a pair of two sites.

On the graphs below MFT curves represent the density along the $y = 0$ line. And MC data is the average over the column. But since the problem is symmetric in transversal direction we expect those densities to be the same.

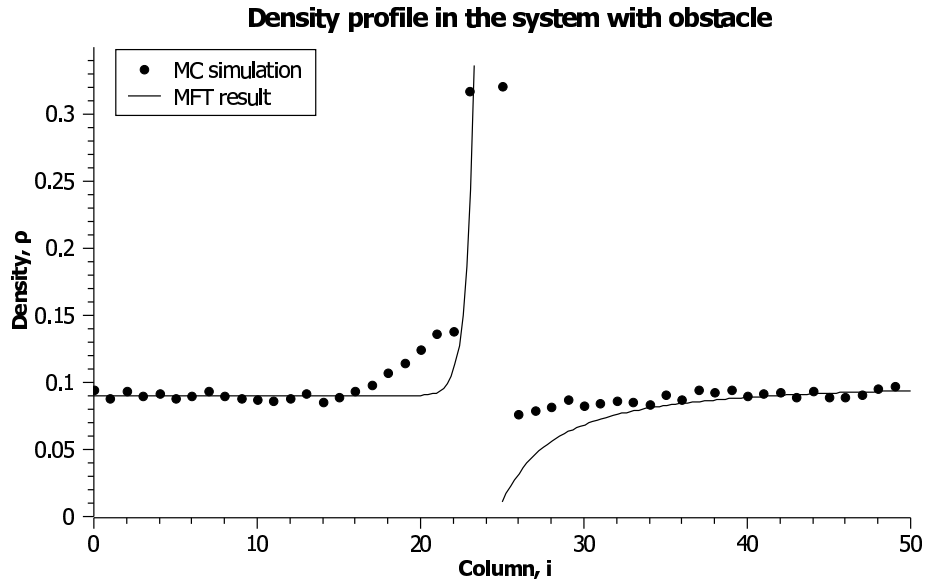

Figure 6.2: Density profiles in the 50x50 lattice with an obstacle.

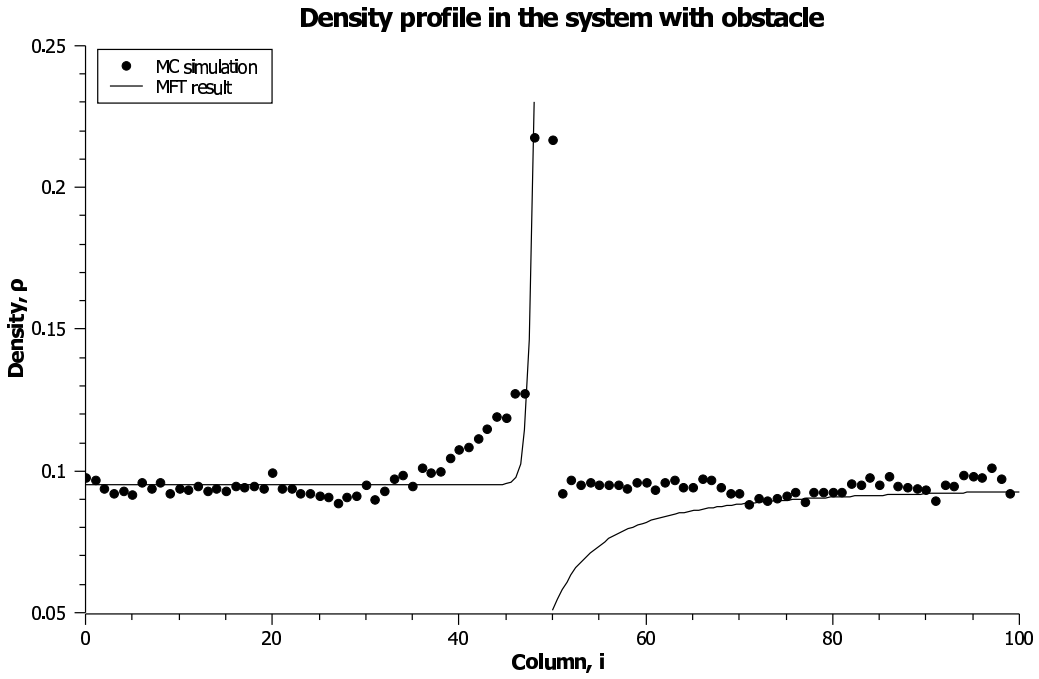

Figure 6.3: Density profiles in the 100x100 lattice with an obstacle.

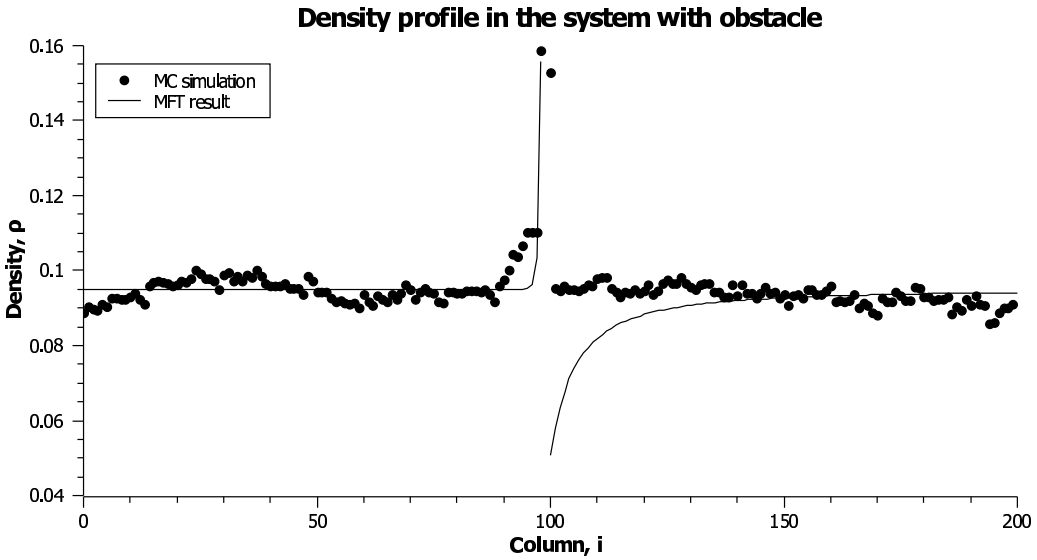

Figure 6.4: Density profiles in the 200x200 lattice with an obstacle.

On all graphs both theoretical and experimental curves show the spike in the middle of the lattice. Results from the simulations repeat the form of the curve given by MFT. When approaching to the obstacle from the left there is a rapid rise of the density. Experimental results show a plateau at the location of the obstacle, whereas MFT doesn't provide the solution at the point of singularity (where the obstacle is located). Behind the obstacle we can observe the decrease of the density to its average value in the system.

Chapter 7

Summary

This work is generalization of the one-dimensional asymmetric simple exclusion process to two dimensions. We introduced a square lattice that is occupied by particels. No more than one particle is allowed to occupy one lattice site. Particles interact by the rule of hard core exclusion. We were considering totally asymmetric process, meaning that the particles can jump only in one direction. Traditionally for this kind of models direction was chosen to be to the right.

First model that we considered was regular two-dimensional ASEP model. Applying mean-field theory assumptions to this model we derived relationship between the current and the density of particles in the lattice (Eq. (3.5)) which contains two kind of terms - current due to the asymmetric drift and current due to the diffusion:

$$j = -\frac{1}{2}\rho' + \rho(1-\rho).$$

MFT for one-dimensional model was developed with additional assumption of the infinite lattice, meaning that the gradient of density in the system is negligibly small. This case is also applicable to our model when we consider the current away from the domain wall which separates high and low density phases in the lattice. This means that we can drop diffusive terms in the expression for the current and we get the same expression that was obtained for one-dimensional model.

Also we obtained expressions for density profiles along the lattice (Eq.(3.8) and Eq.(3.11)):

$$\rho(x) = \frac{1}{2} + \frac{1}{2}\sqrt{1-4j}tanh[(2x-2C)\sqrt{1-4j}],$$

$$\rho(x) = \frac{1}{2} - \frac{1}{2}\sqrt{4j-1}tan[(x-C)\sqrt{4j-1}].$$

They are describing the distribution of the density in the bulk of the system for two different cases: when the current is less then $\frac{1}{4}$ (or the gradient of the density is positive) and when $j \gtrsim \frac{1}{4}$ (gradient of the density is negative) respectively.

To test the MFT for this model Monte Carlo simulations were performed. It was confirmed that dependency of the current on the density of the particles in the system closely resembles the result for the one-dimensional model. Consequently, we can state that depending on the boundary conditions (which dictate the current of the particles in the lattice) system can develop three phases: low density, high density and maximal current phase. The phase diagram for the regular two-dimensional model repeats the one of one-dimensional (Fig. 2.2).

In the model when particle occupies just one lattice site there exists particle-hole symmetry. If we consider flow of the vacancies instead of the flow of the particles, we will get the same expression for $j(\rho)$. Our next problem was to break this symmetry by introducing the particles that occupy more than one site. In our case we've considered two models with particles that occupy two horizontally adjacent and vertically adjacent sites. Using the same mean-field assumptions as for the previous model and assuming that system obeys Poisson statistics we derived dependency of the current on the density of the particles (Eq. (4.8) and Eq. (4.10)).

Using this relationship we constructed a phase diagram for the system with extended particles (for the first model with horizontal particles - Fig. 4.8, 4.9, 4.10; for the model with vertical particles - Fig. 4.14, 4.15, 4.16). On these diagrams one can see that the system still can be found in the three distinct phases - high density, low density and maximal current phases. But also we can observe two significant differences from the regular model. First of all - critical density of the particles is different from the previous value $\frac{1}{2}$ (also the value of the maximal current is different). Another difference is in that fact that the phase separation line no longer has a unit slope, clearly indicating that there is no particle-hole symmetry in the system.

This model was tested by the Monte Carlo simulations.

Regular two-dimensional model also possesses another kind of symmetry - transversal symmetry in distribution of the particles. This effect was achieved by using equal probabilities for the particles to jump upward-right or down-right (and straight right in th model of extended particles) on the lattice sites. And our next step in studying 2D ASEP model was to break this symmetry. In order to do that we made the probability to jump upward-right p different from the probability to jump downward-right $1-p$. Since this change had nothing to do with the motion of the particles in horizontal direction, all results obtained in Chapter 3 for the horizontal component of the current j_x remain true. Under the MFT assumptions expression for the vertical component of the current j_y was derived (Eq. 5.14):

$$j_y = (1-2p)\rho(1-\rho).$$

As it was expected, vertical component of the current depends on the probability to jump up-right. If this probability is equal to 1, all current will go to the negative y direction (with our choice of coordinate system this direction is up). If $p = 0$ we have the current going to the positive y direction or down. Finally, if $p = \frac{1}{2}$, there will be no net drift current in the vertical direction. To verify the results of MFT we ran MC simulation for this model. Results of the simulation (for example, Fig. 5.4 and Fig. 5.5) support the mean-field theory for this model.

The last model that was covered in this work is the model with fixed immovable object (obstacle) in the bulk of the system. The effect of of the obstacle is making the density in the system inhomogeneous. As a consequence, current also will be inhomogeneous. This model is different from one-dimensional model and previously described 2D models in that sense that current in those models was uniform along the system. To study the model a partial differential equation with the dipole source at the origin was constructed (Eq. (6.3)). Solution of this equation gave us an approximation to the spatial distribution of the density in the system with the obstacle (e.g., Fig. 6.2). This solution did not give good result at the point of singularity - location of the obstacle. Also this distribution was obtained by means of MC simulations.

Appendix A. Details of the Monte Carlo Model

In this Appendix we give detailed descriptions of the algorithm used for simulations of each model.

Regular 2D Model

Step-by-step algorithm for regular two-dimensional model:

1. Initialize variables (lattice size - L, number of iterations - ITER, boundary conditions and initial density - p0)

2. Populate lattice with initial density:

```
for i from 0 to L-1
  for j from 0 to L-1
    r = random_number  //from 0 to 1
    if (r < p0) and ((i+j)%2=0) then lattice[i][j] = 1
    // populating only 'black' squares
```

3. Begin iteration cycle

4. Randomly choose a site (with indexes (i, j)).

5. If chosen site is at the left edge of the lattice ($j = 0$):

```
r = random_number //from 0 to 1
if ((i+j) % 2 = 0) and (lattice[i][j] = 0) and (r<=alpha)
   then lattice[i][j] = 1
```

6. If the chosen site is in the bulk of the lattice ($0 < j < L - 1$):

```
r = random_number
nbr_j = j+1 //neighbor column
if r <= 0.5 then
 // jump up
  nbr_i = i-1
```

```
    //periodic boundary conditions
    if nbr_i < 0 then nbr_i = L-1
  //jump down
  else
    nbr_i = i+1
    //periodic boundary conditions
    if nbr_i > L-1 then nbr_i = 0

  if lattice[i][j] = 1 and lattice[nbr_i][nbr_j] = 0 then
     lattice[i][j] = 0;
     lattice[nbr_i][nbr_j] = 1
     current=current+1 //variable to measure current
```

7. If the chosen site is on the right edge ($j = L - 1$):

```
r = random_number //from 0 to 1
if (lattice[i][j] = 1) and (r<=beta)
   then lattice[i][j] = 0
```

8. Every given number of iterations write average value of current to the file

9. Take density measurements every 2-nd MC step during last 200 MC steps. Procedure to measure density:

```
for i from 0 to L-1
   s=0;
   for j from 0 to L-1
     if (lattice[j][i]=1) then s=s+1
   rho[i]=rho[i]+s/(L/2)
```

10. End iteration cycle

11. Write average value of the densities to the file

Regular Model With Periodic Lattice

In order to study the system at the coexistence line we need to make two modifications to the regular model: fix the number of particles so the density is exactly 0.5; and make the lattice periodic. Modified procedure of lattice initialization is following:

```
    np=(L*L/2)*r0) // number of particles
    for i from 1 to np
    {
        // choosing location of the site at random
        i = random_number*(L-1)
        j = random_number*(L-1)
        flag = false;
        while ( flag == false )
            if (lattice[i][j]=0) then
            {
                lattice[i][j] = 1;
                flag = true;
            } else
            {
              i = random_number*(L-1)
              j = random_number*(L-1)
            }
 }
```

And the main body of iteration cycle is as follows:

```
// choosing site at random
j=random_number*(L-1)
i=random_number*(L-1)
// neighbor column with periodic boundary condition
nbr_j=j+1
if (nbr_j>L-1) then nbr_j = 0
```

```
r=random_number
if (r<=0.5)
 {
  //jump up
  if ( ((i-1)>=0) && ((i-1)<=(L-1)) ) then nbr_i=i-1
  if ( (i-1)<0 ) then nbr_i=L-1
 }
else
 {
  // jump down
  if ( ((i+1)>=0) && ((i+1)<=(L-1)) ) then nbr_i=i+1
  if ( (i+1)>(L-1) ) then nbr_i=0
 }



// if the particle at the right boundary
// it will jump to the left edge with probability a
// otherwise probability of jump is 1
if (j == L-1) then prob = a
        else prob = 1

//checking for the jump
r=random_number
if (lattice[i][j]==1) and (lattice[nbr_i][nbr_j]==0) and (r<=prob) then
 {
  lattice[i][j]=0
  lattice[nbr_i][nbr_j]=1
  current=current+1
 }
```

Procedures of taking current and density measurements remain the same as for the regular model.

Extended particles

In this model we modify the algorithm in such a way that we can distinguish between particles. In order to do this we assign each particle a unique identification number. Also we don't have two separate sublattices in this model. Procedure of lattice initialization now looks like following:

```
np=(L*L)*r0) // number of particles
N_part = 0 // id of the particle
for i from 1 to np
{
    // choosing location of the site at random
    i = random_number*(L-1)
    j = random_number*(L-1)
    flag = false;
    while ( flag == false )
        if (lattice[i][j]=0) and (lattice[i][j+1]=0) then
        {
            N_part++;
            lattice[i][j] = N_part;
            lattice[i][j+1] = N_part;
            flag = true;
        } else
        {
          i = random_number*(L-1)
          j = random_number*(L-1)
        }
}
```

At the left edge we need to check that two vertically adjacent sites $(i, 0)$ and $(i, 1)$ (where i is an arbitrary row) are empty before the new particle is attempted to enter the lattice. If the chosen site is in the bulk we need to identify the other half of the particle (it may be to the left or to the right from the chosen site). Here we are using the fact that both halves of the particle have the same id number. Then we attempt

a jump, equally choosing from three possible directions: upward-right, straight right and downward-right. In case of the upward(downward)-right jump we need to check that two target sites are empty. If the particle is attempting to jump straight right, only the site in front of it must be empty.

Procedures of calculating of current and density remain the same. But we must mention that in this case we will measure coverage density (rate of the occupied sites in the lattice).

Vertical Drift Model

Algorithm for this model is modified in such a way that now we have periodic boundary conditions in both directions. We populate the lattice with initial density changing from 0.1 to 0.9 with the step 0.1. Besides, we need to measure vertical and horizontal currents separately.

Procedure of the lattice initialization looks the same as for the regular two-dimensional model. Here we present the main body of the algorithm starting from the iteration cycle. p_up is the probability that the particle will choose upward-right direction of the jump.

```
//choosing the site at random
i = random_number*(L-1)
j = random_number*(L-1)
nbr_j = j+1
if nbr_j > L-1 then nbr_j = 0;
if lattice[i][j] = 1 then
 {
 r = random_number // from 0 to 1
 if r <= p_up then
    // jump up-right
    nbr_i = i-1
    if nbr_i < 0 then nbr_i = L-1
     current_y = current_y-1
     if lattice[nbr_i][nbr_j] = 0 then
      {
```

```
          lattice[i][j] = 0
          lattice[nbr_i][nbr_j] = 1
          current_x = current_x +1
        }
     }
     else
    {
      //jump down-right
      nbr_i = i+1
      if nbr_i > L-1 then nbr_i = 0
      current_y = current_y +1
 if lattice[nbr_i][nbr_j] = 0 then
        {
          lattice[i][j] = 0
          lattice[nbr_i][nbr_j] = 1
          current_x = current_x +1
        }
    }
```

Procedure of writing the current into the file differs only in that fact that now we are recording two values of current: vertical and horizontal components. Procedure of density recording is the same.

Model with the Obstacle

For this model again we are using periodic boundary conditions in all directions. This means that the main body of the algorithm is the same as in the model with vertical bias. The only peculiarity of this algorithm is that we are keeping two particles at the center of the lattice fixed - they can not jump (these particles are forming an obstacle).

Random Number Generator

As a random number generator we are using the function **ran2** from the "Numerical Recipes in C++" [35]. This generator has the period of an order of 2×10^8. In our simulation maximum number of calls to this function occurs in the program for the regular model with 200x200 lattice. The run for this sample is 50 000 MC steps meaning we have $200 \times 200 \times 50000 = 2 \times 10^9$

Technical Details

For realization of the algorithm C++ language was chosen. All programs were compiled by GCC version 4.1. Runs were done under Linux 2.6.17 kernel.

Hardwere employed: PC with AMD Athlon CPU at 2100 MHz ($\approx$ 5935 MIPS) with 512 MB of RAM.

Actual time of the runs:

- 50x50 lattice, 100 000 MC steps: 20 minutes
- 100x100 lattice, 100 000 MC steps: approximately 60 minutes
- 200x200 lattice, 50 000 MC steps: approximately 100 minutes

Bibliography

[1] MacDonald J T, Gibbs J H, Pipkin A C 1968 *Biopolymers* **6** 1

[2] Kukla V *et al.* 1996 *Science* **272** 202

[3] Nagel K, Schreckenberg M 1992 *J. Physique* I **2** 2221

[4] Krug J and Spohn H in *Solids far from Equilibrium: Growth, Morphology and Defects*, Godreche C, ed. (Cambridge University Press, Cambridge, 1991)

[5] Kandel D and Domany E 1990 *J. Stat. Phys.* **58**:685; Kandel D, Domany E and Nienhuis B 1990 *J. Phys. A* **23**:L755

[6] Schütz G *Europhys. Lett.* **48** 6

[7] Shaw L, Zia R K P, Lee K *Phys. Rev. E* **68**

[8] Widom B, Viovy J L, Defontaines A D

[9] Derrida B, Domany E and Mukamel D 1992 *J. Stat. Phys.* **69** 667

[10] Josserand C 1999 *Europhysics Letters* **48(1)** 36

[11] Nagatani T 1994 *J. of the Physical Society of Japan* **63(4)** 1228

[12] http://arxiv.org/pdf/cond-mat/0301398

[13] Cuesta J, Martinez F, Molera J, Sanchez A 1993 *Phys. Rev. E* **48** R4175

[14] Popkov V, Peschel I 200 *J. Phys. A: Math. Gen* **33** 3989

[15] http://arxiv.org/pdf/cond-mat/0310766

[16] Pronina E, Kolomeisky A 2004 *J. Phys. A: Math. Gen.* **37** 2004

[17] Quastel J and Yau H.-T. 1998 *Ann. of Math.* **148** 51

[18] Alexander F, Cheng Z, Janowsky S and Lebowitz J *J. Stat. Phys.* **68**

[19] Huisinga T, Barlovic R, Knospe W, Schadschneider A, Schreckenberg A *Physica A* **294**

[20] Ohira T, Sawatari R *Phys. Rev. E* **58**

[21] http://arxiv.org/pdf/cond-mat/0509546

[22] Burstedde C, Klauck K, Schadschneider A, Zittartz J 2001 *Physica A* **295** 507

[23] Leung K 1994 *Phys. Rev. Lett.* **73** 2386

[24] Dickman R 2001 *Phys. Rev. B* **64** 016124

[25] Sethuraman S 2006 *Alea* **1** 305

[26] http://arxiv.org/pdf/math.PR/0410183

[27] Yau H 2004 *Ann. of Math.* **159** 377

[28] Kolomeisky A B, Shütz G M, Kolomeisky E B and Straley J P 1998 *J. Phys A: Math. Gen* **31** 6911

[29] Scmittman B and Zia R K P *Statistical mechanics of driven diffusive systems*

[30] Lebowitz J L,Presutti E and Spohn H 1988 *J. Stat. Phys.* **51** 841

[31] Derrida B, Evanst M R, Hakim V and Pasquier V 1993 *J. Phys. A: Math. Gen.* **26** 1493

[32] Schütz G and Domany E 1993 *J. Stat. Phys.* **72** 277

[33] Gradshteyn I S and Ryzhik M *Tables of Integrals, Series and Products*, 6th edition, 2000

[34] Bengrine M, Benyouseff A, Ez-Zahraouy H, Krug J, Loulidi M and Mhirech F 1999 *M. J. Condensed Matter* **vol. 2, number 1**

[35] Press W H, Teukolsky S A, Vetterling W T, Flannery B P *Numerical Recipes in C++*, 2nd Edition

Vita

Dmytro Goykolov

February 21, 2007

Date of Birth: September 30, 1980

Place of Birth: Cherkasy, Ukraine

Education

- **State University in Cherkasy**, Cherkasy, Ukraine
  M.S., Physics, 2003

Experience

- **Graduate Teaching Assistant**, University of Kentacky
  Department of Physics and Astronomy,
  2003 - 2007
- **Teacher of Physics**, High School, Cherkasy, Ukraine
  1998 - 2003